Underpainting Recovery using Synchrotron-based X-ray Fluorescence Imaging Data

by

Anila Anitha

B.Tech., University of Kerala 2008

A thesis submitted to the

Faculty of the Graduate School of the

University of Colorado in partial fulfillment

of the requirements for the degree of

Master of Science

Department of Electrical, Computer and Energy Engineering

2010

This thesis entitled:
Underpainting Recovery using Synchrotron-based X-ray Fluorescence Imaging Data
written by Anila Anitha
has been approved for the Department of Electrical, Computer and Energy Engineering

Prof. Shannon Hughes

Prof. Peter Mathys

Prof. Youjian Liu

Date ____________

The final copy of this thesis has been examined by the signatories, and we find that both the content and the form meet acceptable presentation standards of scholarly work in the above mentioned discipline.

Anitha, Anila (M.S., Electrical Engineering)

Underpainting Recovery using Synchrotron-based X-ray Fluorescence Imaging Data

Thesis directed by Prof. Shannon Hughes

Virtual restoration of underpaintings, paintings that have been painted over, has become realizable with data from non-invasive X-ray imaging techniques. With the advent of X-ray synchrotron method, developed by a team in Netherlands [10], it has become possible to collect very high resolution information of the individual chemical composition of any painting in great detail. The large amount of information thus collected can be combined with a variety of image processing algorithms to effectively recover the lost paintings.

In this thesis, we discuss the results of reconstructing underpaintings using X-ray synchrotron datasets of two paintings. The first painting is a Van Gogh and the other a Runge. These paintings are suspected to have been altered by the painters or have an entire underpainting below the surface image, based on traditional X-ray studies. Though previous work on these datasets [7] have yielded visually pleasing results, these algorithms have been painting/scenario specific. This thesis discusses three new methods for the underpainting reconstruction, which focus on delivering a generic and self-sustained solution.

First, a novel approach to source separation is presented to solve the underpainting recovery problem of separating underpainting information from the combined imaging data obtained. We then develop a method for identifying and inpainting areas from which information has been attenuated by particularly thick or X-ray absorbent features of the surface painting. In the end, results from reconstructing the color of the underpainting directly from the X-ray synchrotron imaging data are also presented. This is to our knowledge the first attempt at accurate color reconstruction from such data.

Dedication

To life...

Acknowledgements

I would like to offer special thanks to my advisor Prof. Shannon Hughes, whose patient guidance saw me through this experience. Her constant support helped me make continuous progress, in spite of moving away to Chicago and starting to work full-time. It is her trust and her constant availability, even late on a Sunday night, that kept me motivated to work those long hours in the evenings and weekends. I really appreciate it and consider myself extremely lucky to have had the chance to work under her.

I would like to express my sincere gratitude to Ramesh for his undying patience in motivating me to write this thesis. Without his help, this thesis would not be where it is today. I would also like to thank Prasanna for all his support and technical help with Latex, for listening to my grumblings patiently when I was demotivated, etc.

I would also like to thank Scott Trippel, my manager at Motorola, Chicago, who was very understanding and supportive of my variable hours to meet the thesis work needs.

I would also like to specially thank my dad, mom and Achu who constantly supported and encouraged me to work efficiently and complete my thesis successfully.

Contents

Chapter

1 Introduction 1

1.1 Underpainting Recovery 2

1.2 Data 5

1.3 Signal Processing Challenges for Underpainting Recovery 8

1.4 Overview of Chapters 9

2 Imaging Techniques and Datasets 12

2.1 Imaging and Art 12

2.2 X-ray photography 13

2.3 Infrared Imaging 13

2.4 Ultraviolet Photography 14

2.5 Multispectral Imaging 15

2.6 Spectroscopy 17

2.6.1 Spot X-ray Fluorescence Mapping 18

2.6.2 Synchrotron-based X-ray Fluorescence Spectroscopy 19

2.6.3 Mobile X-ray Fluorescence Spectrometer 19

2.7 Dataset 19

3 Previous Work 25

3.1 Art Reconstruction 25

3.2 Underpainting Recovery 27
3.2.1 Overview 27
3.2.2 Repairing Dataset 27
3.2.3 Registration 28
3.2.4 Source Separation and Identifying Obstructions 30
3.2.5 Inpainting 34
3.2.6 Color Reconstruction 34

4 Source Separation 39
4.1 Synthetic Data 40
4.2 Mutual Information Approach 41
4.3 Conditional Entropy Approach 43
4.3.1 Total Variation Minimization 45

5 Identifying Areas of Information Loss 49
5.1 Enhanced Wavelet Method 49
5.2 Contour Detection 51
5.3 Hue Detection 53
5.3.1 Initial Examination 53
5.3.2 Automatic Hue Detection 54
5.4 Inpainting 58

6 Color Estimation from Chemical Element Data 61
6.1 Ribbon Reconstruction 62
6.2 Hair Reconstruction 64

7 Conclusion 69

Bibliography 71

Figures

Figure

1.1 Surface painting under visible light and superposition of the portrait on it. 3

1.2 X-ray mapping and Infrared photograph of "Pasture in Bloom". 3

1.3 Three different chemical channel images of the painting "Pasture in Bloom" produced via X-ray synchrotron imaging. 4

1.4 Woman's portrait by Philippe Otto Runge. 6

1.5 Surface painting section with corresponding five chemical channel element images for the Runge portrait. 7

1.6 Diagram illustrating the four main subproblems in underpainting recovery. 11

2.1 Detail of a 16th-century Flemish portrait. Black-and-white infrared image reveals preparatory drawing below the paint layer. Figure from Webber in [18] 14

2.2 The marble statue Venus Genitrix in Louvre Museum. Figures from Douma et al. in [11] 15

2.3 The palimpsest under study. On the left is the prayer book and the on the right is the estimated writing of Archimedes under the surface layer. Figure from Salerno et al. in [15] 16

2.4 Multispectral imaging result of the palimpsest. On the left is the palimpsest as seen under visible light and on the right is the same palimpsest under a non-visible wavelength of light. Figure from Salerno et al. in [15] 16

2.5 X-ray Fluorescence Mapping apparatus setup. Figure from Argonne National Laboratory website. 18

2.6 Chemical channels of "Pasture in Bloom" obtained through the synchrotron-based X-ray fluorescence mapping method. 24

3.1 Closer look at the regions where the horizontal shifts are clearly visible. After fixing using a combination of single and dual methods, the region looks visibly continuous. 29

3.2 Horizontal shifts in the raw Sb channel data on the left, after correction gives the image on the right. 29

3.3 Result of registering the channel data to a portion of the surface painting. 30

3.4 Splitting of the channel image into true image and influence image for $\mu = 10$, $\nu = 15$, wavelet = db5, scale = 5 and number of iterations = 80. 32

3.5 The 4 different masks used to inpaint the Sb channel. 35

3.6 Result of inpainting with the 4 masks. 36

3.7 The Van Gogh paintings used for color reconstruction of the underpainting. 36

3.8 Color reconstruction result. 37

4.1 The synthetic data used for the source separation study. 40

4.2 Results of mutual information approach. 42

4.3 Results of conditional entropy approach. 44

4.4 Comparison of the result of the gradient descent approach for the conditional entropy metric with the true separated sources. 44

4.5 Results of total variation minimization modification. 46

4.6 Comparison of the result of the gradient descent approach for the conditional entropy with total variation metric with the true separated sources. 47

5.1 Splitting of the channel image into true image and influence image for $\mu = 10$, $\nu = 15$, wavelet = db6, scale = 5 and number of iterations = 80. 50

5.2 Contour approach results. 52

5.3 Raking light photograph of “Pasture in Bloom” demonstrating thickness of various pigments on surface layer. 55

5.4 Result of simple attenuating hue identification procedure. Hue ranges 0.06 to 0.13 and 0.7 to 1.0 in HSL color space, corresponding to yellow and green respectively, produce a reasonable mask for inpainting. 56

5.5 Results of the automated attenuating hue identification procedure. 57

5.6 Result of inpainting the mask obtained by Automatic Hue Detection Method using the inpainting implementation in [4]. 60

6.1 Results of k-nearest-neighbor estimation of colors from existing available training examples. 63

6.2 Pb and Sb channels of the Runge painting showing clear traces of long hair underneath. 65

6.3 Channel images of the Runge painting’s hand region. 66

Chapter 1

Introduction

Virtual restoration of artwork via image processing is becoming increasingly popular. There are a multitude of valuable artworks that have deteriorated with time. Repair of these artworks is important to restore the original beauty of the art and because these artworks carry a wealth of historical information about the context in which they were created. For example, art historians often study these works in order to better understand the nature of painting at the time of the work's creation, motivations for each painting's creation, the painting's symbolism, the influence of colleagues or teachers on the artist's style, or the historical context in which the painting was created.

The economic, historical and artistic value attached to many of the famous pieces mandates that they remain intact, exactly as they were when they were created. This need to conserve valuable works has led to an interest in non-destructive methods for studying these canvases. These methods allow us to study these pieces without damaging them, allowing us to better understand a particular piece, the artist and his techniques. Hence such non-invasive imaging techniques are increasingly becoming a part of the world of art restoration.

The increasing use of non-invasive imaging and digital photography for archiving digital copies of artworks in museums means that the data needed for virtual restoration of art is now readily available. Image processing techniques can be used together with this data to perform virtual restoration of artwork and gain a picture of what the original artwork might have looked like without damaging the actual piece of art.

As examples of what virtual reconstruction may entail, a variety of things can be done on digital copies of valuable paintings like removing cracks in the paintings, eliminating effects of varnish aging, correcting changes in color of the paintings due to aging, etc. Such digital processing methods are not only used in paintings but also in restoring and archiving various other art forms such as daguerreotypes, frescoes, etc. A more complete review of previous work in the world of virtual reconstruction will be given in Chapter 3.

Despite all these attempts, there is still a large gap between the world of art and the ability of science to conserve/restore it. Many art historians are hesitant to adopt virtual restoration of artwork, compared to other more classical methods of manual restoration. This attitude is because of the large gap between the scientific community and the art world. In foresight, signal processing techniques promise to greatly aid the work of art historians. As will be seen from this work, engineers can complement art historians' prior knowledge and experience with the painter's techniques, with technical expertise in image processing methods to achieve striking results in art restoration efforts.

1.1 Underpainting Recovery

One such interesting art restoration project, which we will focus on in this thesis, is that of recovering underpaintings. Many renowned paintings when subjected to some form of imaging reveal specific forms and shapes under the original surface paintings, suggesting that the surface painting was painted over another painting hidden under it. The reason behind this could be one of many, ranging from financial constraints to changes in style of the painter.

One such work which involves an underpainting, is that of the Dutch artist Van Gogh's painting under his work "Pasture in Bloom" (Figure 1.1). Traditional X-ray imaging revealed faint traces of a woman's head under the surface painting (Figure 1.2).

In a study [17], as many as 20 out of the 130 Van Gogh paintings analyzed were found to contain hidden underpaintings. It is speculated that due to financial constraints, Van Gogh cleared canvases with white layers and used them for painting again. The considerable number of hidden

(a) Surface painting: “Pasture in Bloom” by Vincent van Gogh.

(b) The woman’s portrait shown super-imposed in its location on the surface painting.

Figure 1.1: Surface painting under visible light and superposition of the portrait on it.

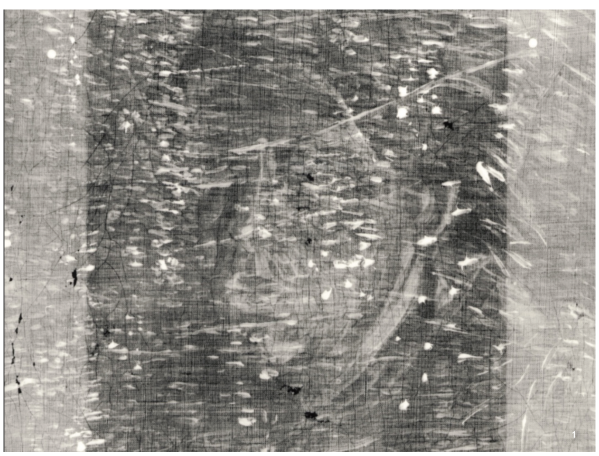

(a) Classical X-ray mapping of a section of “Pasture in Bloom”, showing traces of a woman’s portrait under the surface.

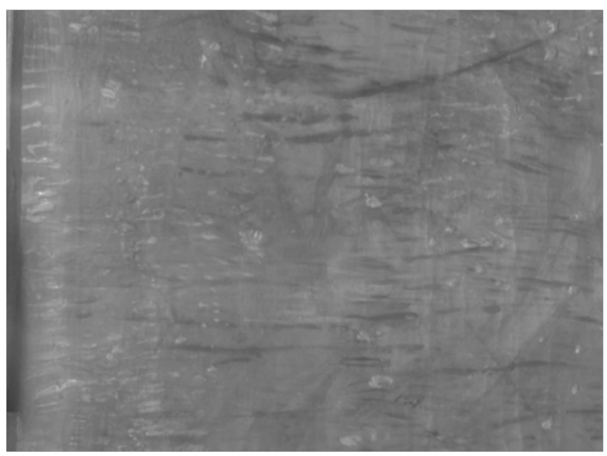

(b) Infrared photograph of a section of “Pasture in Bloom”, again showing traces of a woman’s portrait.

Figure 1.2: X-ray mapping and Infrared photograph of “Pasture in Bloom”.

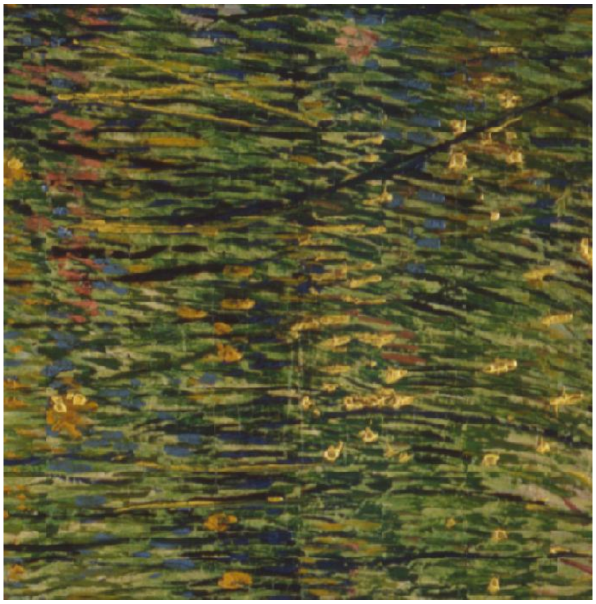

(a) Swatch of the surface image corresponding to the underpainting.

(b) X-ray synchrotron imaging (Fe channel) of the canvas.

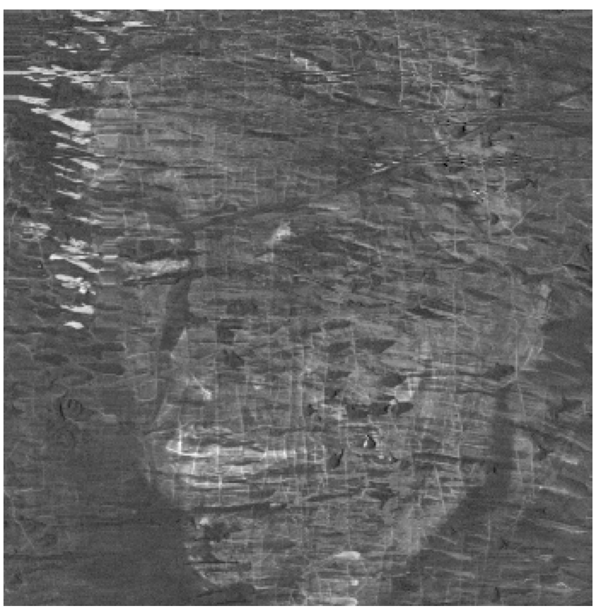

(c) X-ray synchrotron imaging (Hg channel) of the canvas.

(d) X-ray synchrotron imaging (Sb channel) of the canvas.

Figure 1.3: Three different chemical channel images of the painting “Pasture in Bloom” produced via X-ray synchrotron imaging.

works of art indicates the abundance of interesting data available for similar studies. It is vital that the underpaintings be recovered through non-invasive digital reconstruction techniques due to the cost and rarity of the paintings involved. Restoring these hidden works of art would create valuable additions to the current collections in art museums. It would also allow us to gain a better understanding of the life of the painter and his changes in style.

The other painting we will use in this work is one of that of the famous German painter, Phillipp Otto Runge. An imaging study of his portrait of a woman showed that the painting has been altered from its original state. The painting as seen in the surface painting is that of a woman with her hair tied up and wearing a conventional dress (Figure 1.4). But the imaging data shows that the original painting showed the same woman, but with long flowing hair adorned with ribbons. Also the low neckline of the dress in the original painting seems to have been modified to add frills covering the neck (Figure 1.5). These changes could have been made as an afterthought, making the work more suitable to the conservative tastes of Runge's times.

There are many paintings, which have embedded information like these two paintings. The study in this thesis aims at developing a generic framework to study and restore such lost information. The two paintings mentioned above were used to develop the discussed methods.

1.2 Data

Let us take a look at the nature of the data available for the two paintings mentioned above. Synchrotron based X-ray fluorescence mapping was used to generate the data for this study due to the high resolution independent chemical channel information available from it. The X-ray fluorescence data for the Runge painting is shown in Figure 1.5. A detailed review of the conventional imaging techniques used in art restoration projects and the particular method used to obtain data for this thesis can be found in Chapter 2. These various channel data so obtained correspond to specific chemical elements, which gives information about the pigments in that pixel and hence a way to estimate pixel color.

Figure 1.4: Woman's portrait by Phillipp Otto Runge.

(a) Surface image. (b) Co channel data. (c) Fe channel data.

(d) Hg channel data. (e) Pb channel data. (f) Sb channel data.

Figure 1.5: Surface painting section with corresponding five chemical channel element images for the Runge portrait.

1.3 Signal Processing Challenges for Underpainting Recovery

Now, let us look into the signal processing challenges involved in recovering the hidden underpainting using this imaging data of paintings. The process involves 4 sub-steps which will be referred to as Underpainting Recovery Stages 1 through 4. Underpainting Recovery Stage 1 involves correcting acquisition artifacts so that the data is a good representation of the real painting at hand. Underpainting Recovery Stage 2 deals with separation of this corrected data into two sources, one reflecting the surface image and one the underpainting. After the source separation, Underpainting Recovery Stage 3 involves identifying and inpainting areas of information loss. Finally, Underpainting Recovery Stage 4 deals with reproducing the colored version of the painting. The four stages of underpainting recovery are explained below and a comparison of previous work with what is attempted in this thesis is presented. As [7] is the only work available in literature today which deals with these underpainting recovery subproblems, we focus on the results in this paper, examine how successful they were in solving each subproblem, and outline what we will do in this thesis to overcome any shortcomings of this previous work. The underpainting recovery stages are also outlined in the flow diagram shown in Figure 1.6.

Acquisition artifacts are handled in Underpainting Recovery Stage 1. Sometimes, due to timing glitches in acquiring pixel information, there are random horizontal pixel shifts throughout the channel data. Brasoveanu et al. employed a total variation minimization scheme in [7] to solve Underpainting Recovery Stage 1 in eliminating this irregular shifting of lines observed in the acquired image. The approach corrected almost all of these acquisition artifacts in the painting. The same correction method is used for this thesis while dealing with the Van Gogh painting.

Underpainting Recovery Stage 2 deals with source separation. Since the corrected pixel information available contains collective information of both the surface image and the underpainting, the restoration work boils down to separating this information into independent entities. This problem is formally a partial blind source separation problem because partial information from the known surface painting can be used to guide the process. In [7], Brasoveanu et al. attempts to solve Underpainting Recovery Stage 2 using a wavelet approach which did not give very promising results. This thesis pursues a better solution for the same and the efforts along with results are outlined in Chapter 4.

This separated data still contains areas where information has been attenuated by particularly thick or X-ray absorbent features of the surface painting. These have to be inpainted to complete the restoration effectively. In Underpainting Recovery Stage 3, these areas of information loss are identified for inpainting. Brasoveanu et al. in [7], deals with the problem by using many subjective and manual methods, which are highly dependent on the painting under study. This thesis discusses an algorithm which can automatically detect areas of full or partial information loss, thereby allowing for a generic solution to similar problems in recovering lost paintings.

Underpainting Recovery Stage 4 involves estimating color of the restored grayscale painting. Brasoveanu et al. in [7], attempts to color the restored Van Gogh underpainting using information from other paintings of Van Gogh in the same era, lighting, and subject. But they did not use any information from the chemical element data available for estimating colors. Their method also involved a lot of manual intervention based on visual information gathered from the other paintings. Such a method cannot be a candidate for a generic solution to solve color estimation problems. In this thesis a more comprehensive approach to solve Underpainting Recovery Stage 4 based on available chemical element data is presented which is elaborated in Chapter 6 for the Runge painting mentioned before.

Results of attempts to solve the various Underpainting Recovery Stages by Brasoveanu, et al. in [7] and by this thesis are presented in Chapter 3 and the following chapters respectively.

1.4 Overview of Chapters

The thesis is arranged as follows. Chapter 2 explores the various imaging methods used for noninvasive study of art work. Chapter 3 presents description of previous work in the field of art restoration in general followed by a detailed description of a particular work, [7], in the field of underpainting recovery. This study provides a perspective for the work presented in the next chapters. Chapter 4 discusses the source separation methods used to separate the surface painting attributes from the underpainting details. Chapter 5 details the methods developed to identify areas of information loss and inpainting results for these artifacts. Chapter 6 describes in detail the color estimation method we have developed. Chapter 7 concludes the thesis by summarizing the efforts explained in all chapters.

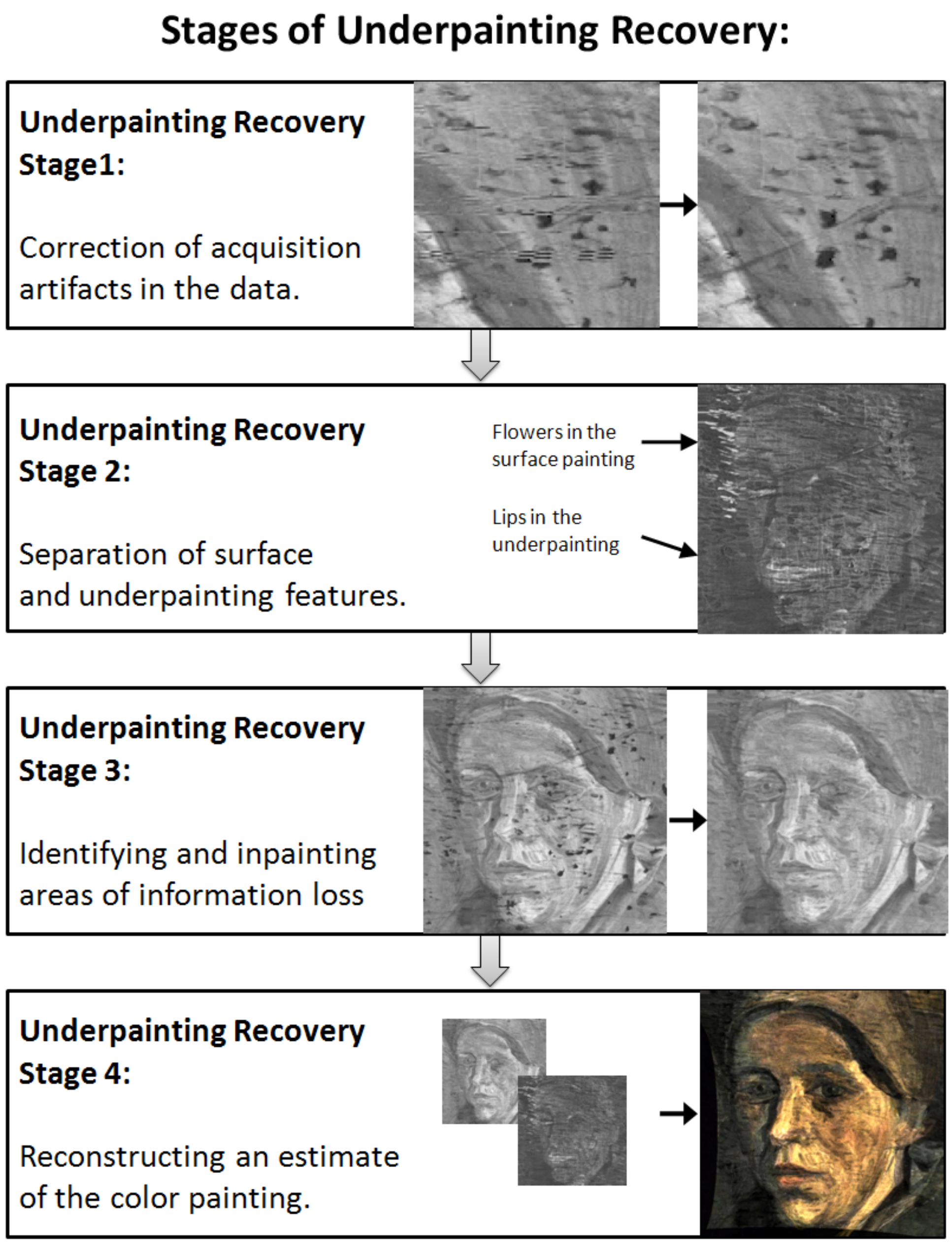

Figure 1.6: Diagram illustrating the four main subproblems in underpainting recovery.

Chapter 2

Imaging Techniques and Datasets

Imaging is a term used to represent a wide range of methods that are used to create, preserve or duplicate images. This term can denote a variety of things ranging from visible-light photography to electron microscopy.

2.1 Imaging and Art

Imaging has long been used to examine a painting's underlayers in the study and conservation of art. As early as the late nineteenth century, radiographic methods such as Xray photography were used in art conservation, and they are still used widely today. Later, spectroscopic methods, used individually or as in combination with other methods, began to provide a better non-invasive way of imaging invaluable art. With technological advances, many more types of spectroscopic methods like that of infrared (IR) photography, ultraviolet (UV) photography, multispectral imaging, synchrotron-based Xray fluoresence imaging, etc. are starting to be used in art conservation and restoration efforts.

This chapter provides an overview of the most common spectroscopic methods followed by a closer look at the larger field of spectroscopy. Then, the X-ray synchrotron fluorescence method is described in detail along with a study of its newer and better variations. This is followed by a brief description of the data used in this thesis, which was obtained using a novel X-ray synchrotron fluorescence mapping.

2.2 X-ray photography

With the gaining popularity of X-rays, towards the end of 20th century, even museums started investing in X-ray sources for use in preserving art forms. X-ray photography is generally done by scanning a painting with X-rays and capturing these radiations on a photographic plate on the back side of the painting. While passing through the painting, X-rays are absorbed along the way based on the pigments they are passing through. Different chemicals absorb X-rays at different levels; for example, the white pigment lead absorbs almost all of the X-rays and does not let this radiation pass through it. Thus by studying the concentration of X-rays collected on the photographic plate, the amount of X-rays absorbed can be found and thus the chemicals it passed through can be deduced.

2.3 Infrared Imaging

Another method which caught on after the X-rays was infrared (IR) imaging. The main difference between X-ray and IR is that IR does not penetrate the painting fully. Hence information regarding inner layers of a painting will be collected. This is a good source of studying underlying images or initial sketches made by an artist before starting to paint, known as underdrawings. Art conservators use IR imaging to obtain details about the intermediate underdrawings in a painting, which gives information regarding the preparatory phase of a painting.

IR imaging, which is based on absorption spectroscopy, uses electromagnetic spectrum in the infrared region. It exploits the fact that molecules absorb certain frequencies that are characteristic of their structure and hence can be identified uniquely. The IR rays, being a non-emission-based spectroscopy, do not get reflected by the surface layer of the painting and penetrate deeper. Thus layers of alteration in the painting that are not uncovered by emission spectroscopic methods, can be studied in detail, by analyzing IR spectroscopic results. As an example, a study of a 16th century Flemish portrait [18] using IR imaging reveals a preparatory drawing under the surface painting as shown in Figure 2.1. This type of imaging can thus be helpful in deciding whether a painting is the

(a)

(b)

Figure 2.1: Detail of a 16th-century Flemish portrait. Black-and-white infrared image reveals preparatory drawing below the paint layer. Figure from Webber in [18]

prime version by the original artist or a copy, and whether it has been altered by over-enthusiastic restoration work.

2.4 Ultraviolet Photography

Ultraviolet (UV) light photography deals with imaging objects under ultraviolet frequencies of the electromagnetic spectrum. When UV radiations are incident on an object, various kinds of fluorescence can occur depending on the subject under study. The radiation emitted by the substance can be used to uniquely identify it. In the world of imaging art, they are used in a multitude of ways. For example, in a study of the life-size marble statue Venus Genitrix in Louvre

(a) Under visible light.

(b) Under UV light.

Figure 2.2: The marble statue Venus Genitrix in Louvre Museum. Figures from Douma et al. in [11]

Museum under UV light, some parts of the statue were found to be unoriginal. This suspicion can be verified by observing Figure 2.2. The statue's hand looks similar to the rest of its body when studied under visible light. But under UV light, the hand section fluoresces more, indicating that this section could have been a later replacement. UV light imaging is also used to reveal erased signatures, detect retouches made during restoration, spot forged sections, etc. in paintings.

2.5 Multispectral Imaging

Multispectral imaging captures image information at specific frequencies across the electromagnetic spectrum. It can allow extraction of additional information that the human eye might not capture with its limited color reception. A noteworthy example of the application of this imaging technique in restoration is its use in the Archimedes Palimpsest project as detailed in [15]. A Christian monk is believed to have recycled the parchment in an Archimedes book which is believed

Figure 2.3: The palimpsest under study. On the left is the prayer book and the on the right is the estimated writing of Archimedes under the surface layer. Figure from Salerno et al. in [15]

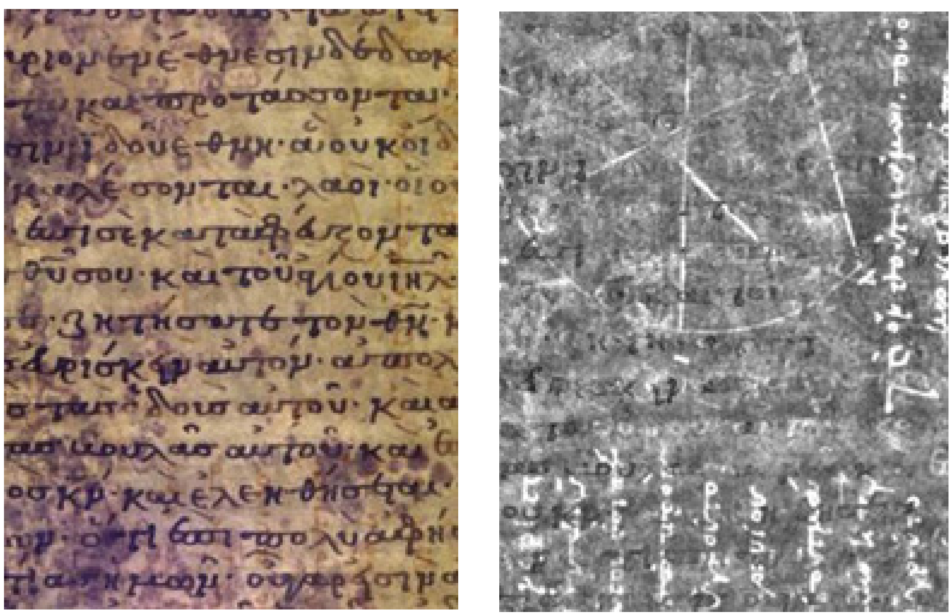

Figure 2.4: Multispectral imaging result of the palimpsest. On the left is the palimpsest as seen under visible light and on the right is the same palimpsest under a non-visible wavelength of light. Figure from Salerno et al. in [15]

to contain explanations about calculus. This could prove that Archimedes was indeed the inventor of calculus, long before Sir Isaac Newton. However, the monk's recycling turned the Archimedes book into a new prayer book. In Figure 2.3, it can be observed that there is a layer under the surface writing which is of a different orientation. On close study, it was confirmed to be of another language too. By studying the parchment under multispectral light, scholars were able to confirm that the prayer book was indeed written over an Archimedes book on calculus. In Figure 2.4, it is evident that multispectral imaging method has revealed the Archimedes book of calculus under the prayer book and this high quality data can be used for research in recovering the original Archimedes parchment.

2.6 Spectroscopy

Before studying X-ray fluorescence spectroscopy in detail, let us understand what spectroscopy is in general. Interaction of radiation with matter can result in absorption, scattering, and/or reemission (in different wavelength) depending on the nature of radiation as well as the molecular structure/energy-state of the responding matter. The nature and quantum of energy transfer taking place in the process can reveal certain physical properties of the material. Such physical properties known as the spectral properties, are unique and thus can be used as identifying signatures. Spectroscopy is the technique of using changes in the electromagnetic radiation (in the form of absorption, emission, or scattering) during interaction with a material for the purpose of understanding its properties.

Spectroscopy can be classified broadly on the nature of the interaction as absorption spectroscopy, emission spectroscopy and scattering spectroscopy. Electromagnetic energy when incident on a material triggers one of the following actions: absorption, emission or scattering, depending on the nature of the object. The resulting spectrum is unique and can be analyzed to study the nature of the matter. Hence spectroscopy is widely used for any kind of non-invasive imaging needs.

Though X-ray is used for imaging purpose in general, for the specific purpose of non-invasive study of art works, IR and multispectral imaging are also prevalent as was explained in Sections 2.2, 2.3 and 2.5.

2.6.1 Spot X-ray Fluorescence Mapping

When X-rays of sufficient energy interact with a substance, excitation of inner shell electrons in the atom to outer empty orbitals occur; sometimes leading to complete removal of them (ionization). The "hole" created by the excited electron will then be filled by outer orbital electrons. This de-excitation process releases energy in the form of radiation (fluorescence). The energies in the various emission frequencies are characteristic of a specific atom. X-ray absorption and emission spectroscopy are widely used in chemistry to determine chemical bonding and elemental composition.

With a suitable apparatus, these characteristic X-ray frequencies can be measured. A typical layout for a X-ray fluorescence microprobe is illustrated in Figure 2.5. The incident X-rays excite

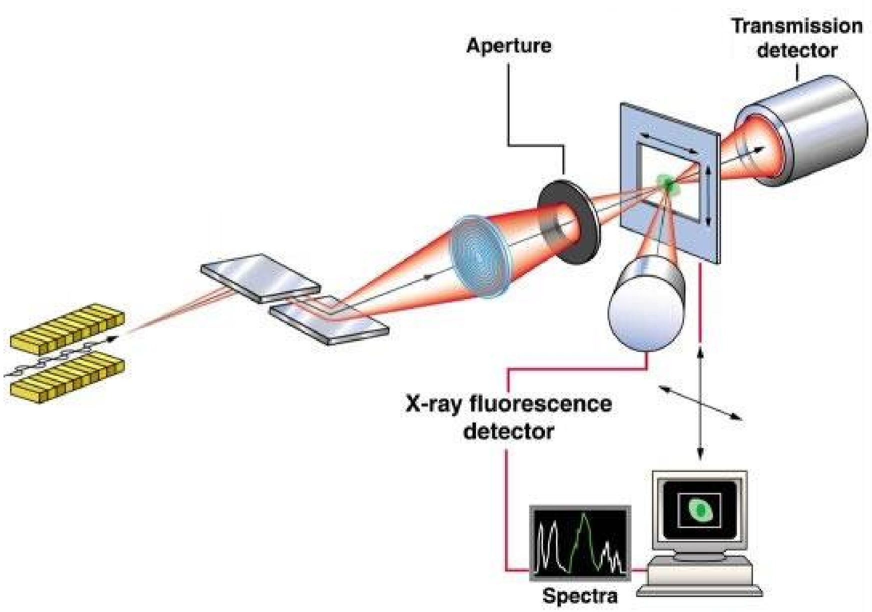

Figure 2.5: X-ray Fluorescence Mapping apparatus setup. Figure from Argonne National Laboratory website.

photo electrons in the sample resulting in fluorescence emission. The excess energy carried away by the emitted photons can be detected using a detector system. By measuring the number of electron-hole pairs generated by the emitted photons, the chemical element from which it originated can be deduced. Since the number of detected fluorescence photons depends directly on the quantity of material present in the illuminated spot of the sample, the amount of material can be quantified easily. This method of quantifying the amount of material based on the fluorescence caused by X-ray radiations on a sample is referred to as X-ray fluorescence mapping. Typically, this mapping is performed for almost 10 elements simultaneously at each scan position.

Spot X-ray Fluorescence is mostly used for taking spot readings from paintings to identify the pigments present in a specific spot.

2.6.2 Synchrotron-based X-ray Fluorescence Spectroscopy

X-ray Fluorescence Spectroscopy was used very frequently in the world of art, to analyze only a spot of the artwork. It was hard to use the method for imaging a larger area. Dr. Joris Dik in [10] introduced a revolutionary method in which an entire image can be scanned. A synchrotron-based light source is used for this purpose which produces high energy X-rays enabling higher quality readings. This new method gives the possibility of imaging larger areas in a good resolution.

2.6.3 Mobile X-ray Fluorescence Spectrometer

Work is still underway under the guidance of Dr. Joris Dik to build a smaller system that would replace the enormous and expensive synchrotron device currently used to produce X-ray fluorescence mapping data of scanned paintings. This system would greatly increase the ease of obtaining imaging data as opposed to the synchrotron method which involves transporting very expensive paintings across the globe to the synchrotron site. In the current version of the mobile imager, results are stated to be much noisier than the traditional method. But cleaning the data using image processing techniques can be used to extract useful information from the noisy data.

2.7 Dataset

The unique experimental setup in Section was used to map various chemical compositions of the two paintings under study in this thesis work. The Van Gogh's "Pasture in Bloom" was imaged for 14 chemical channels, representing Arsenic (As), Barium (Ba), Bismuth (Bi), Cadmium (Cd), Cobalt (Co), Chromium (Cr), Copper (Cu), Iron (Fe), Mercury (Hg), Manganese (Mn), Lead (Pb), Antimony (Sb), Strontium (Sr), and Zinc (Zn) as in Figure 2.6. It can be seen that the chemical elements correspond to specific pigments in the painting; antimony corresponds to naples yellow color, mercury to vermillion red, cobalt to cobalt blue, lead to lead white, etc. They give comprehensive information about the spatial and chemical (color pigment) composition of the painting. Most of the channels contain the surface painting information, but some channels have vivid residue from the underpainting. For instance, Channel 12, the antimony channel, is the most prominent one.

Runge's dataset has 5 data channels each corresponding to Co, Fe, Hg, Pb and Sb as shown in Figure 1.5. It can be observed that some of the channels have clear information about the painting before it was modified. The presence of ribbons in the woman's flowing hair, probably of the same color as her waist ribbon, can be observed in the cobalt and mercury channels. Also the lead, iron and antimony channels clearly capture her longer hair. It can also be observed in the antimony and iron channel that the woman could have been wearing a dress with a lower neckline.

This thesis aims at developing automated methods to recover underpaintings using the data from the synchrotron based X-ray fluorescence method.

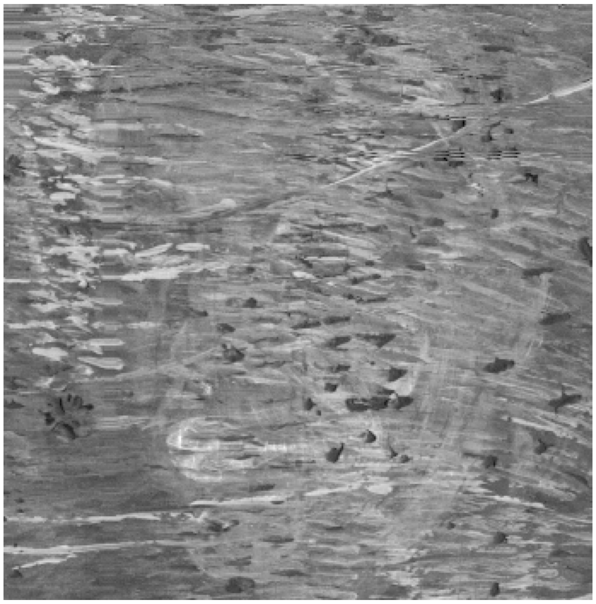

(a) As Channel.

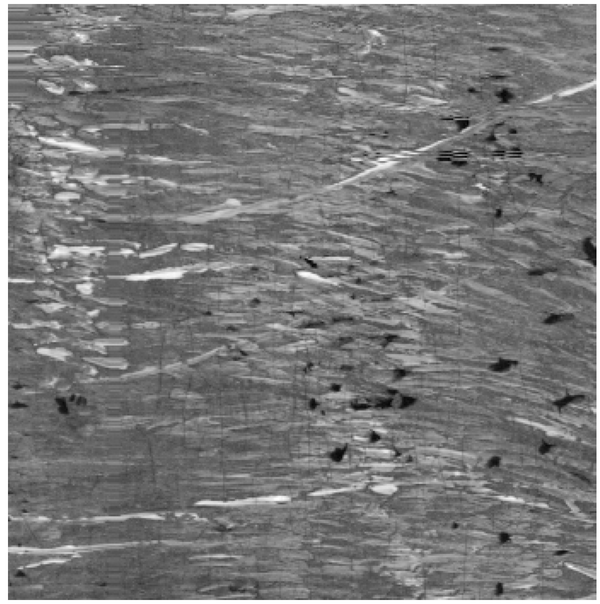

(b) Ba Channel.

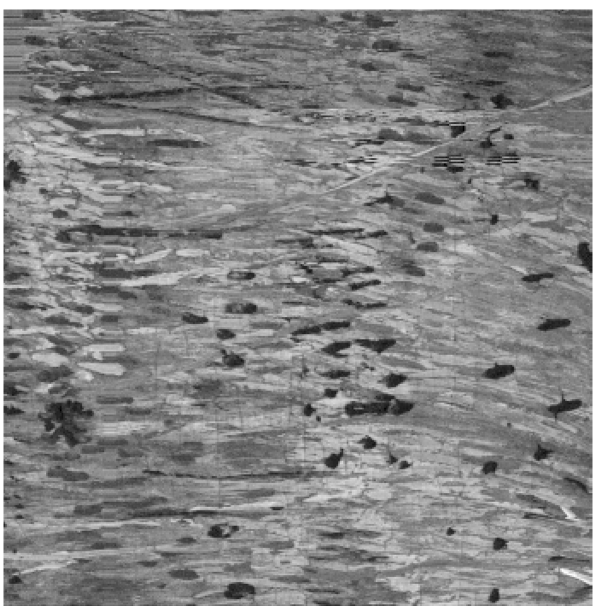

(c) Bi Channel.

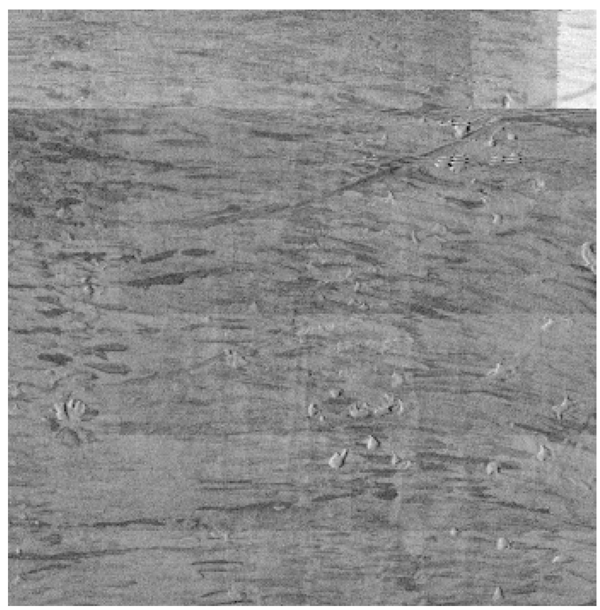

(d) Cd Channel.

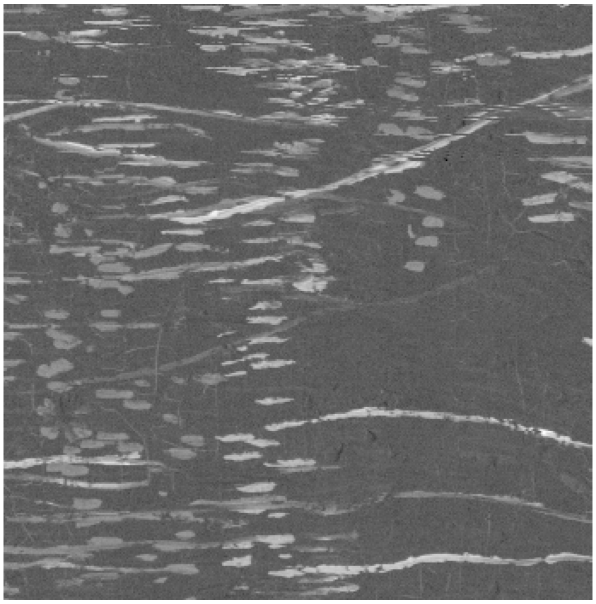

(e) Co Channel.

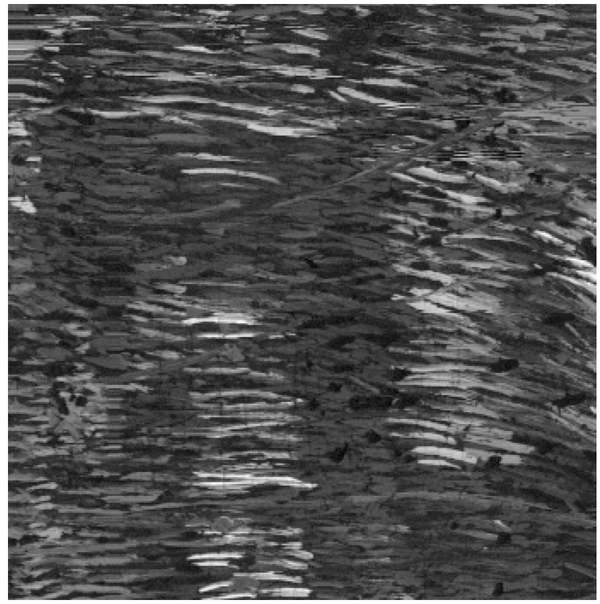

(f) Cr Channel.

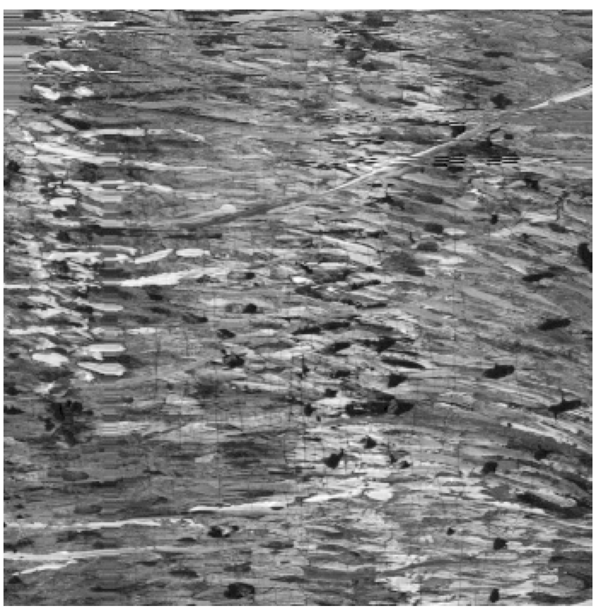

(g) Cu Channel.

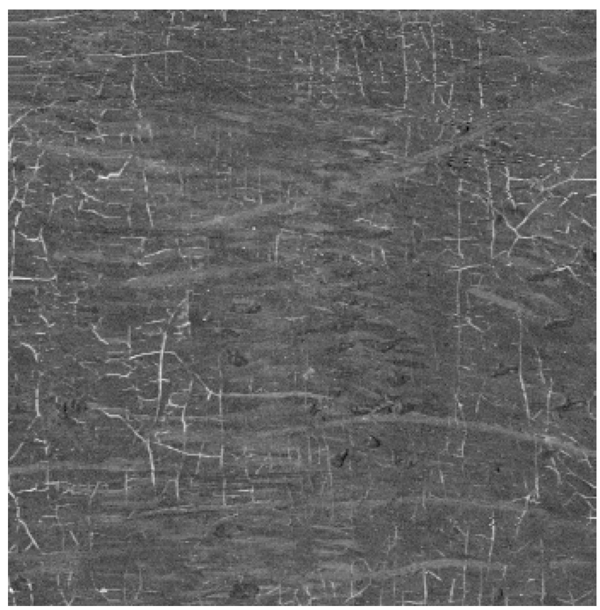

(h) Fe Channel.

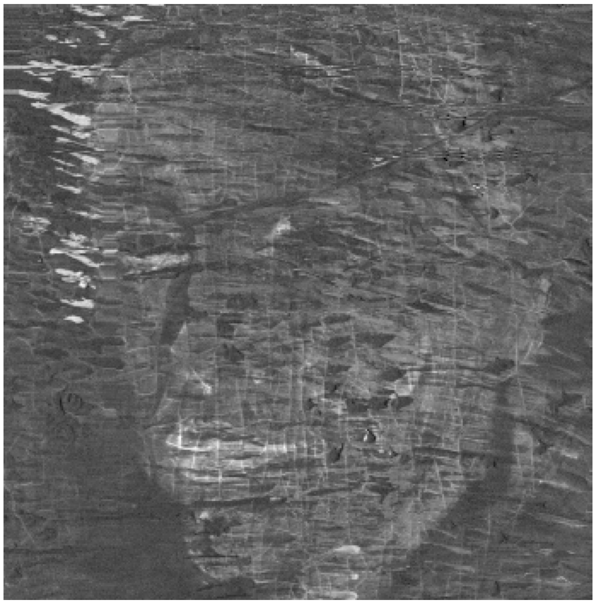

(i) Hg Channel.

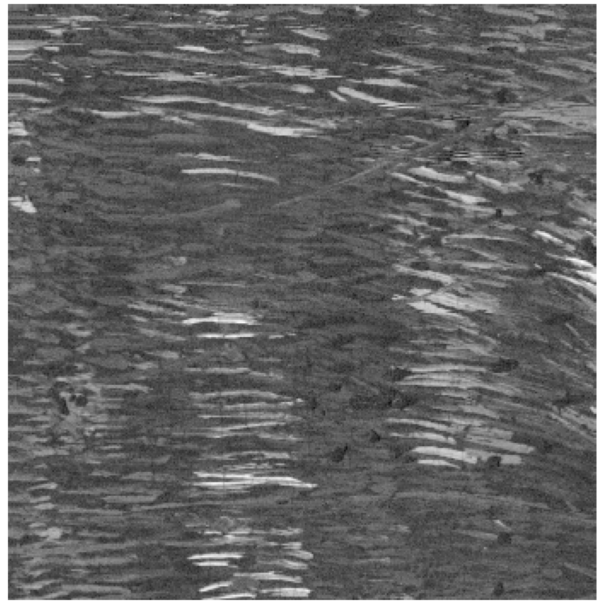

(j) Mn Channel.

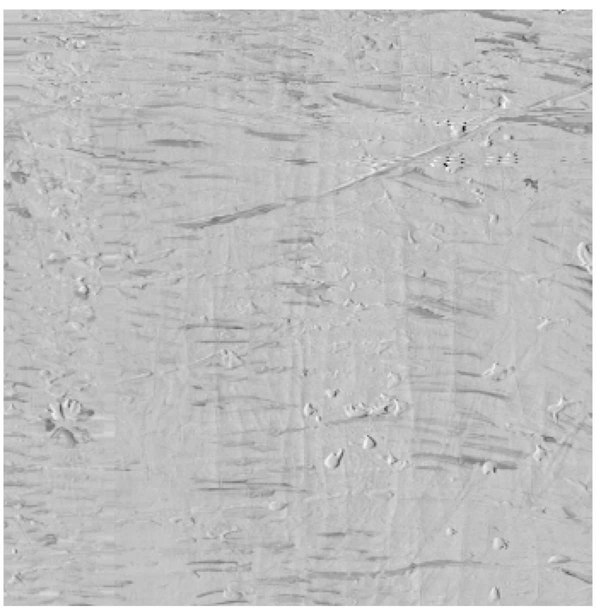

(k) Pb Channel.

(l) Sb Channel.

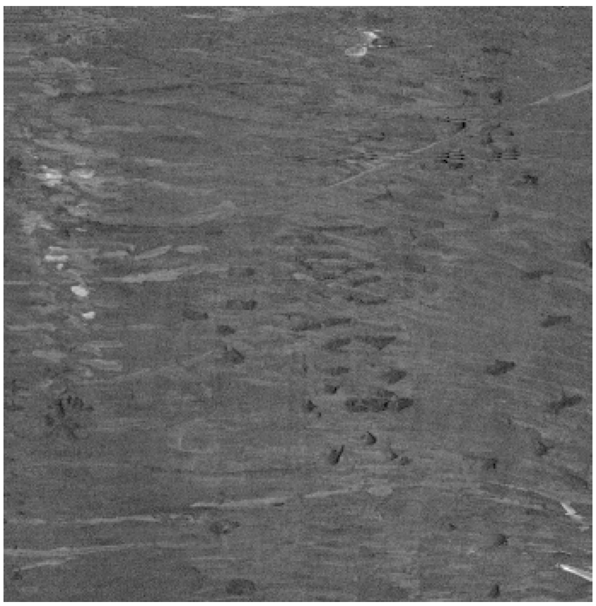

(m) Sr Channel.

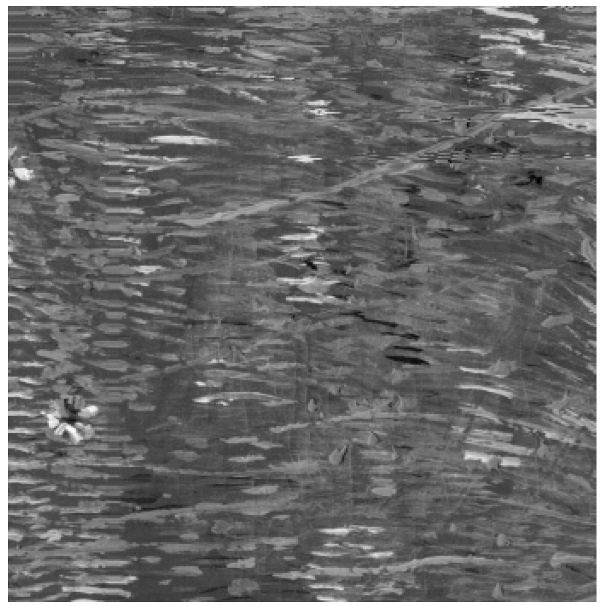

(n) Zn Channel.

Figure 2.6: Chemical channels of "Pasture in Bloom" obtained through the synchrotron-based X-ray fluorescence mapping method.

Chapter 3

Previous Work

The beginning of this chapter presents the current literature in virtual art reconstruction techniques. This is followed by a detailed discussion of Brasoveanu et al. [7], which according to our knowledge, is the only previous work in the field of underpainting recovery.

3.1 Art Reconstruction

Virtual restoration of artwork via image processing has gained importance in recent times. Digitization of art work and paintings enables important non-invasive conservation and restoration efforts. These digitized works can be processed to provide a variety of restoration treatments. Geometric aberrations, introduced by the imaging process, for example, can be nullified by doing simple processing on the digital copy. Cracks formed due to aging can also be treated in the digital copy of a painting. The crack patterns in the original imaged data can in fact be used for dating or studying damages caused due to transportation. Imaged data is also useful for mapping pigments in paintings. An overview discussing the scope of image processing in the preservation of art pieces is presented in [13] and [14].

Techniques for virtually annotating and restoring various other art forms such as daguerrotypes and frescoes are also being widely used. Daguerrotypes are exquisite gold-coated silver-mercury amalgams on a silver plate. These rare pieces are not reproducible. Conservation of existing daguerrotypes is a very delicate task as even the gentlest of handling can destroy the original work. The need for non-invasive imaging techniques gains relevance here due to the sensitivity of daguerrotypes to physical restoration processes. In [16], techniques for annotating and restoring the daguerrotype, “The Cincinnati Panorama” using its massive gigapixel digital image, are presented.

Data from frescoes are mostly spread across various modalities like Ultraviolet spectroscopy, IR spectroscopy, etc. Registration of these different data is a very important preprocessing step in the conservation of frescoes. After processing the registered information in these modes, fusion of this multimodal information provides valuable information to guide the restoration process. The non-invasive analysis of frescoes can be very helpful in recovering and conserving the historic artforms. In [6], restoration efforts on a badly ruined fresco from a 11th century church in the Slovak Republic, are discussed.

In general, signal processing methods on imaged art data are used to perform a variety of functions. The data can be denoised and processed to produce a high resolution result which can be very useful in increasing the content quality of the images. One such application is explained in greater detail in [2].

Another important application used in virtual reconstruction is color reconstruction. By modeling the variations in absorption and scattering properties of paint surface pigments due to aging and applying the reverse transformation, the effect of aging can be cancelled digitally. Such a reversal to the aging effect of the surface hues on Seurat’s painting “A Sunday on La Grand Jatte”, is attempted in [3].

Also, the coloring of a painting provides a lot of information about the painting. Changes or fades in color can be used for dating the works of art. Studying the pigment composition of a painting using multispectral imaging methods can provide an insight into the artist’s working style. One such extensive study on Vincent van Gogh’s *The Starry Night* for pigment mapping of pixels is elaborated in [19].

Virtual art reconstruction is growing to be a very accepted solution for valuable pieces of art. The large number of successes stand testimony to this. But the specific field of underpainting recovery is still nascent with only one known paper that reports research in the field. The ideas presented in this paper are elaborated in the following section.

3.2 Underpainting Recovery

Brasoveanu et al., [7], is the only available detailed study on reconstructing underpaintings from synchrotron based X-ray fluorescence data. A part of this thesis is an extension to this work and focuses on automating the identification of areas of information loss for inpainting. This section provides the required background about the work in [7] which will help us understand this thesis in the coming chapters.

3.2.1 Overview

In [7], X-ray fluorescence data from the novel synchrotron method, as detailed in Chapter 2, of a Van Gogh painting "Pasture in Bloom" is studied to recover the portrait of a woman which was found hidden beneath the surface painting. The raw data had acquisition artifacts which had to be fixed to make the data usable. The corrected chemical channels thus obtained had to be registered accurately with the part of the surface painting which contained the underpainting, to facilitate good reconstruction results. After performing these preprocessing steps, various artifacts present in the channel images had to be identified and eliminated. Finally, the gray scale image of the underpainting had to be digitally colored to obtain a realistic 'lost and reconstructed' painting. In [7], Brasoveanu et al. develop each step of this process to arrive at a visually appealing result in the end. The important steps in [7] and intermediate results are shown in the sections below.

3.2.2 Repairing Dataset

Data from all the channels of the painting were observed to have horizontal shifts that seemed to be randomly distributed in the 2D image space. These seemingly arbitrary shifts (Figure 3.1) displayed some regularity which could be used to characterize them. The appearance of a shift in a pixel was always accompanied by monotonic horizontal shifts in the nearby pixels. But the location of these pixels in a horizontal line seemed to vary randomly across different rows. The shifts were due to a pixel level phenomenon and hence did not look like anything that could have been intentionally created by a real painter. So these errors were categorized as digital acquisition/representation errors. Their presence could be explained by acquisition timing errors while collecting the pixel data. It was confirmed by consulting Dr. Joris Dik that these timing error artifacts could exist, given the acquisition process. The painting is normally scanned each row at a time by illuminating each pixel with light and staying at that pixel until information is collected. There were some pixels which took longer time, which lead to the subsequent shifts for every pixel after it. This process explains the monotonic increase after the shifting begins. Also, this timing glitch could happen anywhere along the row and hence the occurrence of the shift seems random in a particular line. Understanding the nature of the shifts helped in fixing it.

Brasoveanu et al. used a total variation minimization approach across horizontal lines of the acquired image to fix these acquisition errors in the channel data. Details of the implementation are explained in [7].

Also, it was seen that all the channels suffered from the same shifts. Hence the correction algorithm was first applied to antimony channel which had the most visual data of the portrait of the woman underneath. Brasoveanu et al. in [7] state that there were residual shifts after the above process and recommended manual intervention to clear these. After visual verification of the results, the same processing was applied to the rest of the channels.

This section explains Brasoveanu et al. solving the Underpainting Recovery Stage 1 problem in a visually satisfactory way. The same repaired dataset (Figure 3.2) is used for this thesis work as well.

3.2.3 Registration

To continue processing the channel image with respect to the original surface image, they have to be registered closely. If not, it will affect every other step in further processing. The original surface painting is a larger image which is a digital photograph. But the channel image is a part of the original image which is acquired from an imaging process. They are not expected to have a

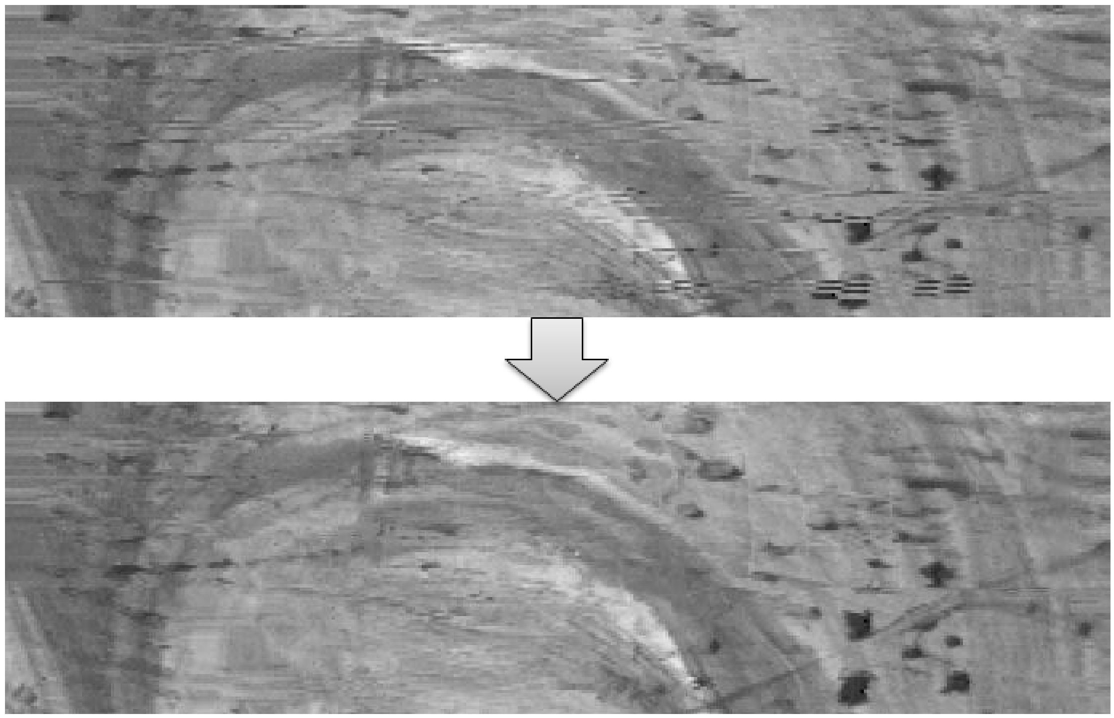

Figure 3.1: Closer look at the regions where the horizontal shifts are clearly visible. After fixing using a combination of single and dual methods, the region looks visibly continuous.

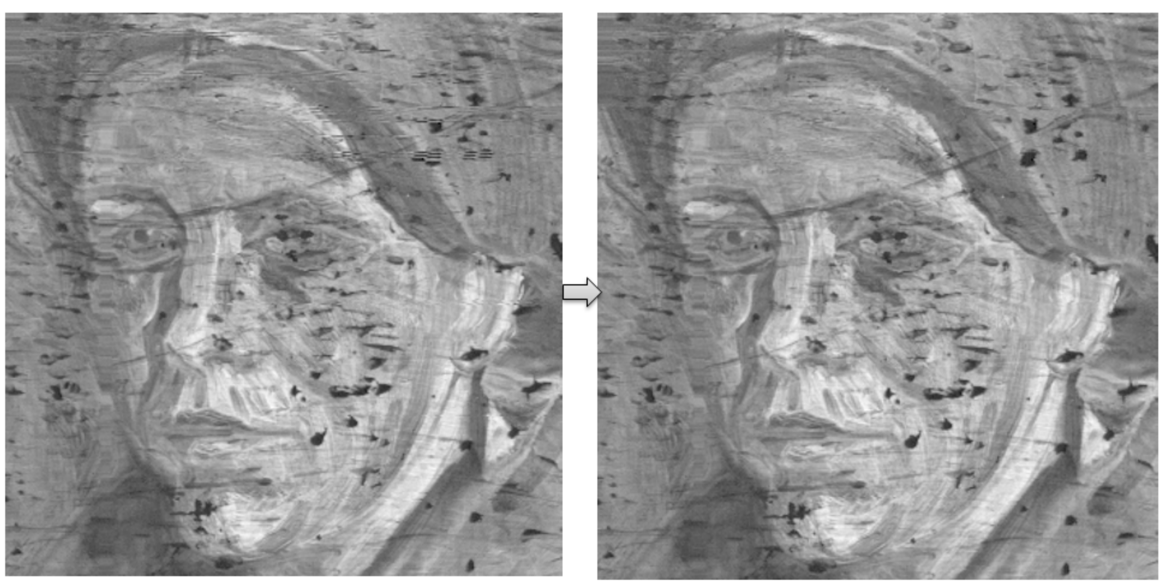

Figure 3.2: Horizontal shifts in the raw Sb channel data on the left, after correction gives the image on the right.

one to one correspondence as such. But a good registration is highly necessary which was achieved in [7] by considering the model of 'non-parametric discrete constrained two-dimensional warping'.

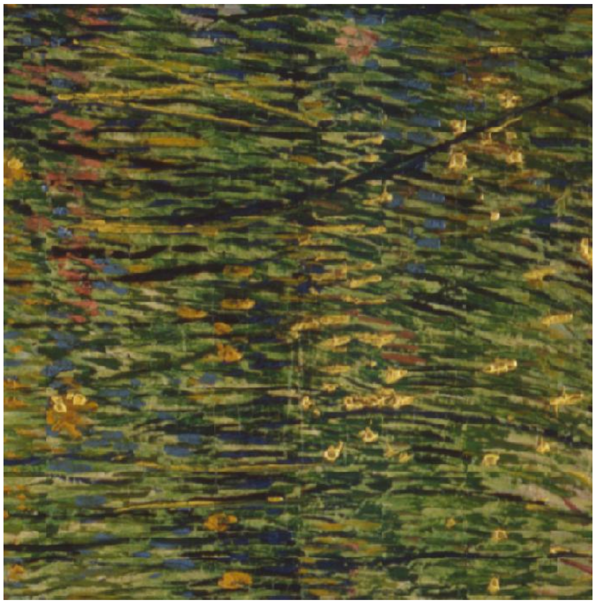

(a) Registered portion of surface painting.

(b) Sb channel data registered with the surface painting

Figure 3.3: Result of registering the channel data to a portion of the surface painting.

The registration is performed by the following four steps - feature detection, feature matching, transform model estimation and image transformation. Feature detection is done by choosing salient features in the channel image like corners, contours, etc. which is matched with the surface image features. This mapping is used to estimate a transform model. The image is transformed thus to register the two images as close to each other as possible (Figure 3.3).

Very good registration results were obtained in [7] and the same data is exported for use in this thesis too.

3.2.4 Source Separation and Identifying Obstructions

3.2.4.1 Source Separation

Due to the difference in palettes for the surface image and underpainting of the van Gogh painting, the sources are almost already separated. The surface painting used bright colors to depict the scenery and the underpainting contained mostly sober colors in the portrait. Hence the different chemical channel information referred to either the surface image or the underpainting and never a mixture of both of them, for most of the channels. For example, the antimony channel almost entirely reveals the underpainting. Due to this independence of channel information, source separation was not focused on much in [7]. However, the data will usually not be pre-separated in this way. Hence a source separation algorithm has to be developed in a generic approach to underpainting recovery (Underpainting Recovery Stage 2). Such an attempt in this thesis is elaborated in Chapter 4.

3.2.4.2 Identifying Obstructions

A close look at the channel images shows many holes (black pixels with no useful chemical data) that imply a loss of information after imaging. In the case of the antimony channel which has a lot of underpainting details, black blob- and blade-shaped holes were seen on the face of the woman's portrait. These holes could be places where the presence of some pigments absorbed all X-rays passing through them, leaving behind no trace of information about these areas. To recover the original underpainting, it is necessary that these obstructions be identified and inpainted. Brasoveanu et al. attempted a wavelet approach to solve the problem.

The channel images have combined information about the surface image and the underpainting. The percentage of each constituent in every channel is different depending on which pigment is most represented by the channel. For example, the antimony channel has most of the underpainting information with very little influence from the surface image. This imbalance is probably because antimony is found in the Naples Yellow pigment which is used mostly in creating flesh-like shades and hence the portrait has a lot of that pigment. Also the surface painting being a very bright and colorful scene, has almost none of the pigment. For this reason, this is the channel chosen for further processing to allow us to get to the underpainting as quickly as possible. However, even the small influences of the surface image on this channel data have to be removed to totally recover the underpainting.

The wavelet approach attempts to separate the channel image into two components, a true underpainting image and a second image depicting the influences of the surface image upon it. In terms of wavelet coefficients, the wavelet transform of the antimony channel $\mathcal{C}(\lambda)$ is modeled as the sum of the wavelet coefficients of the true underpainting image $\mathcal{T}(\lambda)$ and the wavelet coefficients of the influence image $\mathcal{I}(\lambda)$.

$$\mathcal{C}(\lambda) = \mathcal{T}(\lambda) + \mathcal{I}(\lambda)$$

The source separation was formulated as a minimization problem as given below,

$$\sum |\mathcal{C}(\lambda) - (\mathcal{T}(\lambda) + \mathcal{I}(\lambda))|^2 + \mu \sum \phi(\lambda)|\mathcal{I}(\lambda)|^2 + 2\nu \sum |\mathcal{T}(\lambda)|$$

where μ, ν are weights for the second and third term respectively and $\phi(\lambda)$ is the following weighting function

$$\phi(\lambda) = \left(1 - \frac{\mathcal{B}(\lambda)}{\beta}\right)^+$$

(a) Fixed, registered channel image.

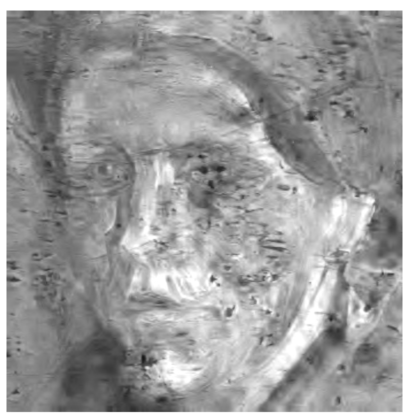

(b) True Image.

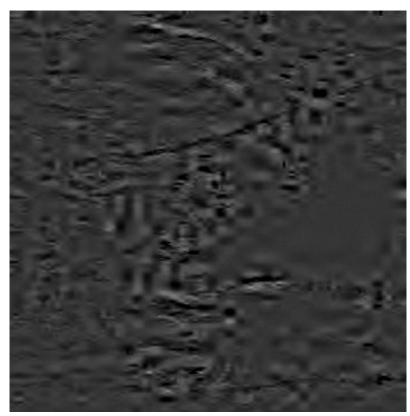

(c) Influence Image.

Figure 3.4: Splitting of the channel image into true image and influence image for $\mu = 10$, $\nu = 15$, wavelet = db5, scale = 5 and number of iterations = 80.

Here $()^+$ denotes the positive part of the variable inside brackets, $\mathcal{B}(\lambda)$ represents the wavelet transform of the grayscale version of “Pasture in Bloom” and β refers to the 99th percentile of the distribution $\mathcal{B}(\lambda)$ (top 1% of the largest wavelet coefficients). It is evident that $\phi(\lambda)$ is almost 1 when the surface image wavelet coefficients are small and vice versa. This dependence penalizes the second term in such a way that when the wavelet coefficients are small in the surface image, the coefficient is separated out as the true image/underpainting component and when wavelet coefficients are large in the surface image (edges like in flowers and grass blades), the coefficient is separated out as an influence image component.

The first term forces a final solution with the true and influence images approximately adding up to the total image. The third term penalizes if the image is not sparse in wavelets like a real image and hence guides the solution to arrive at a real world image.

The minimization can be solved to arrive at the following set of equations:

$$\mathcal{T}_n(\lambda) = \mathcal{S}_\lambda(\mathcal{C}(\lambda) - \mathcal{I}_n(\lambda))$$

$$\mathcal{I}_{n+1}(\lambda) = \frac{\mathcal{C}(\lambda) - \mathcal{T}_n(\lambda)}{1 + \mu\phi(\lambda)}$$

where $\mathcal{S}_\nu$ is a thresholding function defined as

$$S_\nu(x) = \begin{cases} x - \nu & \text{if } x > \nu \\ x + \nu & \text{if } x < -\nu \\ 0 & \text{if } |x| \leq \nu \end{cases}$$

These can be solved iteratively for n iterations, to get the source separation as shown in Figure 3.4. It can be seen that the blobs got partially diminished with their boundaries being replaced with surrounding data. But the loss of detail and sharpness due to repeated application of the wavelet transform and its inverse is very obvious to the naked eye.

In attempting to solve the Underpainting Recovery Stage 3 problem of identifying obstructions for inpainting, Brasoveanu et al. tried a wavelet approach which did not give satisfactory results. A different approach for solving Underpainting Recovery Stage 3 more efficiently is presented in Chapter 5 of this thesis.

For the rest of the restoration process in [7], Brasoveanu et al. relied on obstructions identified by a method involving subtraction of the grayscale value of the underpainting from the grayscale value of the surface image. This was because it was observed that the dark blobs corresponded to bright regions on the surface image. Selection of a mask for inpainting was broken down into pieces for better manageability of the inpainting process. In their work, Brasoveanu et al. identify 4 kinds of masks - blobs, lines, artifacts and the eye (Figure 3.5). The blobs and blades masks were identified mostly by the subtraction method. The artifacts remaining after the first two masks were identified manually to form the other two masks for general artifacts and obstructions around eye.

In this thesis, an algorithm is proposed to identify the obstructions more comprehensively. The developed method is also automated to detect these artifacts and is painting independent.

3.2.5 Inpainting

The identified obstructions have to be filled in for full or partial loss of information in these places. An inpainting mask was created by identifying the obstructions and then inpainting was done. Brasoveanu et al. use an exemplar based algorithm, implemented by S. Bhat [5] based on [15], for their work.

The exemplar algorithm when applied on this comprehensive mask provided a visually plausible inpainting. The result recovered the gray scale portrait of the lady to a good level of satisfaction (Figure 3.6), and did not increase the blur of the image. But on closer evaluation, it can be observed that fine brush strokes and contours are not continued. It is not very evident, but continuation of these lines could have produced a result closer to the original underpainting. In this thesis, another inpainting implementation based on Bertalmio et al. [4] which carries through isophotic lines is presented in Chapter 5.

3.2.6 Color Reconstruction

To reconstruct the color of the original underpainting, two Van Gogh paintings of similar subjects painted from similar angles in Van Gogh's Neunen period were studied. They are *Head of a Peasant Woman* held at the Kröller-Müller Museum in Otterlo, Netherlands and *Peasant Woman in a White Cap* held at the Vincent van Gogh Museum, Amsterdam, Netherlands [9] (Figure 3.7).

To use the information from the two available similar paintings and color the grayscale

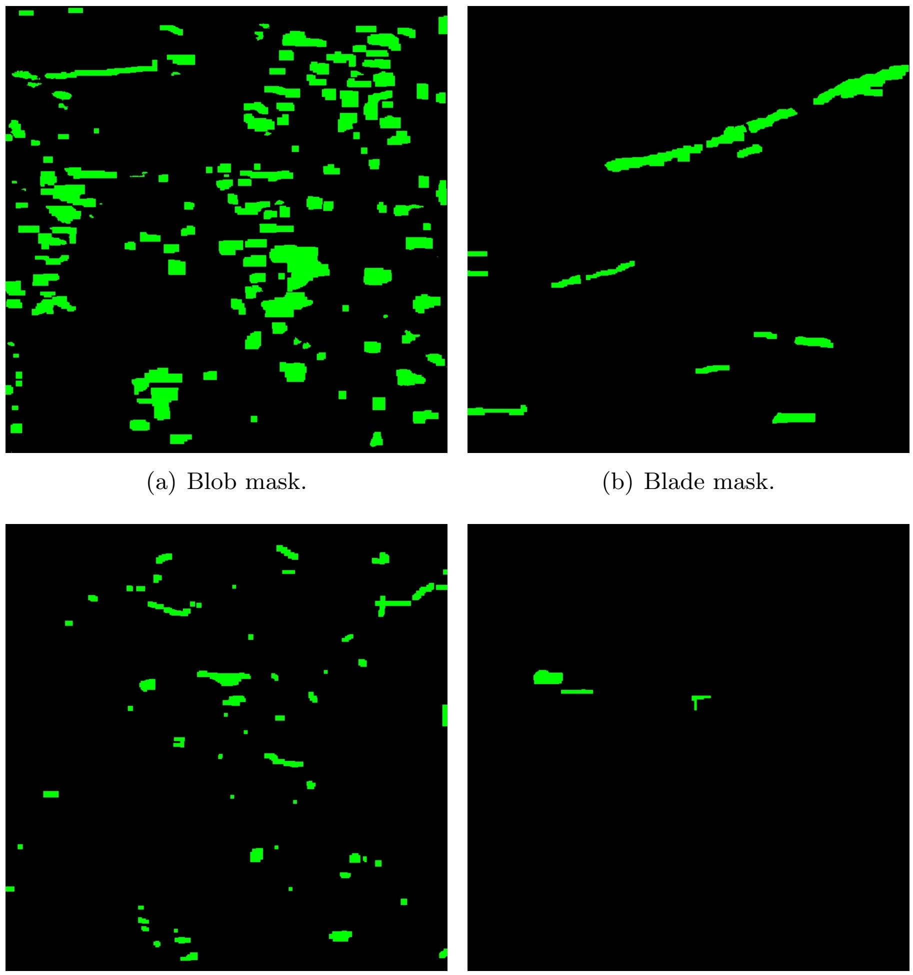

(a) Blob mask.

(b) Blade mask.

(c) Artifact mask.

(d) Eye mask.

Figure 3.5: The 4 different masks used to inpaint the Sb channel.

Figure 3.6: Result of inpainting with the 4 masks.

(a) *Head of a Peasant Woman*, Kröller-Müller Museum, Otterlo, Netherlands.

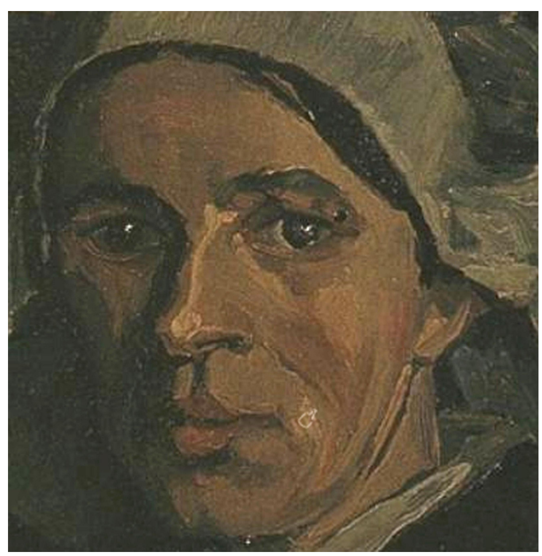

(b) *Peasant Woman in a White Cap*, Vincent van Gogh Museum, Amsterdam, Netherlands.

Figure 3.7: The Van Gogh paintings used for color reconstruction of the underpainting.

Figure 3.8: Color reconstruction result.

underpainting, the paintings have to be in close correspondence to the underpainting. Hence the two paintings in color, were cropped and morphed so that the facial features in these portraits would align with the facial features of the woman in the underpainting. A combination of the color information from the two paintings, was then taken, to capture the gradation in hue and tone.

It is believed that the underpainting was closer to the Amsterdam painting than the Otterlo one. So a weighted average of the two paintings' chromatic information was used to color the inpainted antimony channel. A luminance map of the antimony channel itself was used as the luminance values for the final colored image. With a weighting factor of 75% for the Amsterdam painting and 25% for the Otterlo one, the chrominance value for the final colored image (Figure 3.8) is taken as a weighted average of the two painting's chrominances.

Thus for Underpainting Recovery Stage 4, Brasoveanu et al. developed a very crude method which was also dependent on the presence of other similar paintings. The method also depended on manual adjustments. Such a solution is not generic and cannot be reused for solving future underpainting recovery problems.

Unlike in the previous work, in this thesis, a generic solution to the problem of color reconstruction for underpaintings is attempted, which does not involve any manual intervention and uses information from the different chemical channel data to perform the coloring. This algorithm is developed using data of a Runge painting which was altered. A machine learning approach is used to recover the original painting and its color information.

In summary, it is evident that [7] has been an interesting first work and has set a good precedent for development of interesting new algorithms. But the results of solving Underpainting Recovery Stages 2, 3 and 4 call for better and more efficient methods, which are attempted in this thesis in the upcoming chapters.

Chapter 4

Source Separation

This chapter discusses attempts to solve Underpainting Recovery Stage 2, which deals with source separation. Source separation consists of solving a highly under-determined system. A of data from surface image and underpainting forms the chemical channel's information. The only available information that can be used to separate the individual components out is the known visible light photograph of the surface image which never is of the same imaging modality as the combined chemical channel data. The problem is clearly under-determined as it involves splitting a set of chemical element images into twice as many sources with only one image of side-information.

The data model in pixel space is constrained by

$$\begin{cases} \mathcal{C}_{ch} = \mathcal{C}_{surf} + \mathcal{C}_{under} \\ \mathcal{C}_{surf}(x, y) > 0, \forall\ x, y \\ \mathcal{C}_{under}(x, y) > 0, \forall\ x, y \end{cases}$$

where $\mathcal{C}_{ch}$ is the combined information of both components in the chemical channel data that we have measured, and $\mathcal{C}_{surf}$ and $\mathcal{C}_{under}$ are the sources corresponding to the surface and underpaintings respectively that we would like to split $\mathcal{C}_{ch}$ into. The first condition makes sure that the component images add to form the total image. The second and third conditions restrain the resulting components to be non-negative.

The source separation can be framed as an optimization problem. The metric for optimization should be selected carefully to enable proper separation. The motive in source separation is to separate the combined image into its two source components, the surface image component, $\mathcal{C}_{surf}$, and the underpainting component, $\mathcal{C}_{under}$. Ideally the surface image component should be as close to the original surface painting, $\mathcal{I}_{surf}$, as possible and the underpainting component should be in no way related to the available surface painting. This problem can be framed as

$$\max[M(\mathcal{I}_{surf};\mathcal{C}_{surf}) - M(\mathcal{I}_{surf};\mathcal{C}_{under})]$$

$$\text{constrained on} \qquad \begin{cases} \mathcal{C}_{ch} = \mathcal{C}_{surf} + \mathcal{C}_{under} \\ \mathcal{C}_{surf}(x,y) > 0, \forall\ x,y \\ \mathcal{C}_{under}(x,y) > 0, \forall\ x,y \end{cases}$$

where $M(X;Y)$ is a similarity metric between the images X and Y.

We attempt to solve this partial blind source separation problem by finding a suitable metric in the following sections.

4.1 Synthetic Data

To develop a satisfactory solution for the source separation, initially we work on some fabricated data for which we know the ground truth. The data model is that we have two sources on top of each other in unknown proportions to get one image for each chemical element.

(a) Source 1 - Grayscale image of Lena

(b) Side information - Visible light photograph of Lena

(c) Source 2 - Grayscale image of Peppers

(d) Mixture.

Figure 4.1: The synthetic data used for the source separation study.

This chapter uses a combination of standard images (Lena and Peppers) as shown in Figure 4.1. They are mixed in the ratio of 1:1 initially. Note that, to mimic the real source separation problem we face, we will have as our side-information a color image, so that it is from a different imaging modality than our sources.

The color Lena image is used as the known side information we have, to frame the source separation problem. The mixture serves as the combined chemical channel data. The objective is to deduce the original Peppers image (source 2) from the mixture available.

4.2 Mutual Information Approach

To measure the closeness of two images, different metrics like direct correlation or distance measures can be used, if the two images are of the same modality. But in the case of multimodal images, a metric which measures how much knowledge of one image conveys information about the other one is required. The source separation dealt with here involves multimodal images and hence such mutual information is chosen to be the required metric.

Mutual information between two variables is a measure of how much knowing one of the variables reduces the uncertainty about the other. In a way, it is a measure of how one variable relates to the other, so that the knowledge of one can convey information about the other. Knowing this, we can safely assume that the mutual information between the surface image and the component of channel data corresponding to the surface image should have high mutual information. Also, the component involving the underpainting details should ideally have high mutual information with the original underpainting and zero mutual information with the surface image.

Thus, we may use mutual information as the similarity metric mentioned above. We will attempt to maximize mutual information of the surface component with the surface image while minimizing the mutual information of the underpainting component with the surface image. This gives the optimization problem:

$$\max[I(\mathcal{I}_{surf};\mathcal{C}_{surf}) - I(\mathcal{I}_{surf};\mathcal{C}_{under})]$$

(a) Separated source 1 - estimated surface image component.

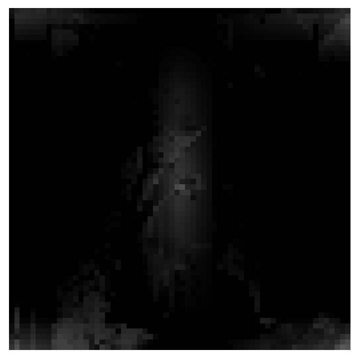

(b) Separated source 2 - estimated underpainting component.

Figure 4.2: Results of mutual information approach.

$$\text{constrained on} \qquad \begin{cases} \mathcal{C}_{ch} = \mathcal{C}_{surf} + \mathcal{C}_{under} \\ \mathcal{C}_{surf}(x,y) > 0, \forall\ x,y \\ \mathcal{C}_{under}(x,y) > 0, \forall\ x,y \end{cases}$$

where $I(X;Y)$ is the mutual information between random variables X and Y.

To find the solution to this optimization problem, we shall first try a gradient ascent algorithm. To maintain the coherence of each image, we adjust its wavelet coefficients to increase the objective function's value (subject to the constraints) instead of using gradient ascent on the pixel values directly. The gradient ascent algorithm was run iteratively on entire images with varying step size in each iteration. The results obtained are as shown in Figure 4.2. It can be observed that the source separation was not complete and that one image became brighter and the other darker after many iterations. The algorithm seems to have figured that by making one image bright and one image completely dark it would increase the overall uncertainty of one and decrease the overall uncertainty of the other, resulting in higher mutual information for the first term of the objective function and lower mutual information for the second term. Hence, this solution solves the maximization problem without actually performing the intended source separation. To avoid this problem, the following variation to this idea was attempted.

4.3 Conditional Entropy Approach

To overcome the problem in the previous approach, the metric can be changed to a percentage of uncertainty explained by the surface image. This can be expressed in terms of conditional entropy as

$$H(Y|X)/H(Y)$$

where $H(Y|X)$ is the conditional entropy of random variable Y when X is known. Mutual information and conditional entropy are closely related. The mutual information $I(Y;X)$ measures how much the entropy of Y is reduced if X is already known. This can be expressed as

$$I(Y;X) = H(Y) - H(Y|X)$$

(a) Separated source 1 - estimated surface image component.

(b) Separated source 2 - estimated underpainting component.

Figure 4.3: Results of conditional entropy approach.

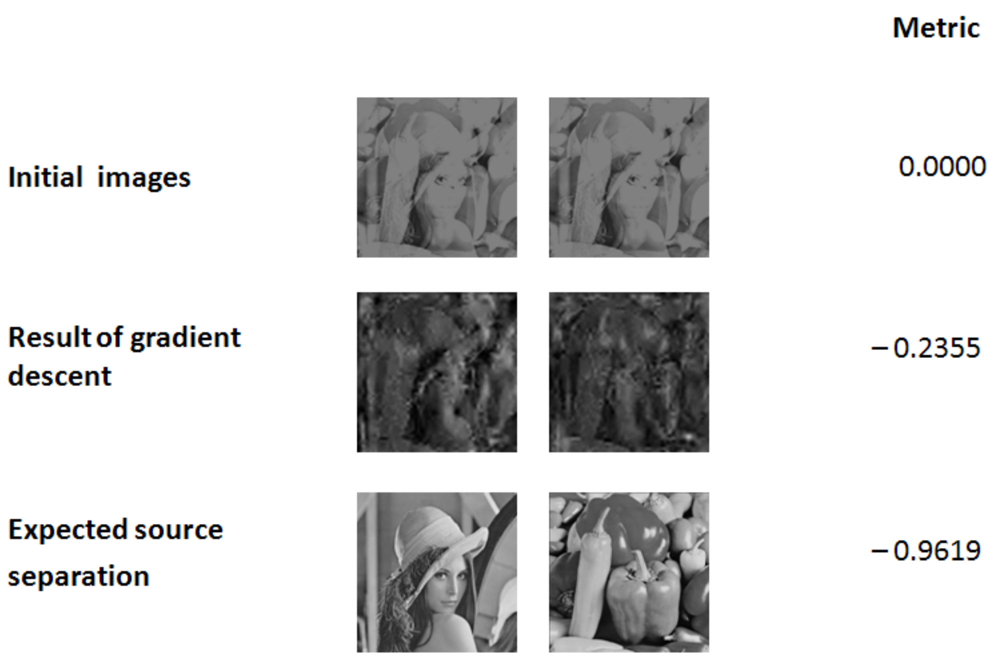

Figure 4.4: Comparison of the result of the gradient descent approach for the conditional entropy metric with the true separated sources.

Since the values are entropy, the metric should be minimized here, rather than maximized as in the case of mutual information. Thus, modified problem is:

$$\min \left[\frac{H(\mathcal{C}_{surf}|\mathcal{I}_{surf})}{H(\mathcal{C}_{surf})} - \frac{H(\mathcal{C}_{under}|\mathcal{I}_{surf})}{H(\mathcal{C}_{under})} \right]$$

$$\text{constrained on} \qquad \begin{cases} \mathcal{C}_{ch} = \mathcal{C}_{surf} + \mathcal{C}_{under} \\ \mathcal{C}_{surf}(x,y) > 0, \forall\ x,y \\ \mathcal{C}_{under}(x,y) > 0, \forall\ x,y \end{cases}$$

We attempt to find the solution to this optimization problem via gradient descent. The results of the gradient descent algorithm are shown in Figure 4.3. It can be observed that now the results do not show the separation into brighter and darker images. The algorithm seems to have started separating the sources, but does not converge finally to the expected separation. They seem to be stuck in some kind of local minima along the way. We can verify that the algorithm has not fully converged to the global minimum via a comparison of our final solution attained via gradient descent with the true separated sources (see Figure 4.4). Gradient descent results in a final objective function value of -0.2355 while the true sources if separated properly would produce an objective function value of -0.9619. Clearly, the gradient descent gets stuck and stops a long way from the true global minimum.

Also, it can be observed that the partially separated sources are not very smooth. The smoothness of the resulting images can be improved by including another term in the objective function, as explained in the following subsection.

4.3.1 Total Variation Minimization

To increase the smoothness of the results obtained above, a penalty term was added to the objective function to encourage it to find smooth images instead of non-smooth images wherever possible. The term added was the total variation of the estimates of surface and underpainting components.

Total variation (TV) is a measure of how much the function changes value. A total variation minimization on an image produces an image with fewer oscillations/ripples, without sacrificing the image's sharp edges. TV of an image $f(x, y)$ is an integral of the norm of the gradient over the whole image:

$$\iint ||\Delta f||\, dxdy$$

Notice that the total variation is a sum of the magnitudes of the image's gradient vectors at each point. This is very much the L1 norm of the gradients. Hence, minimizing the total variation leads us to a L1 norm minimization of its gradients, and hence produces a result with few edges which looks like a real world image.

(a) Separated source 1 - estimated surface image component.

(b) Separated source 2 - estimated underpainting component.

Figure 4.5: Results of total variation minimization modification.

By adding the penalty term, the optimization problem now becomes

$$\min \left[\frac{H(\mathcal{C}_{surf}|\mathcal{I}_{surf})}{H(\mathcal{C}_{surf})} - \frac{H(\mathcal{C}_{under}|\mathcal{I}_{surf})}{H(\mathcal{C}_{under})} + \lambda TV(\mathcal{C}_{under}) + \lambda TV(\mathcal{C}_{surf}) \right]$$

$$\text{constrained on} \qquad \begin{cases} \mathcal{C}_{ch} = \mathcal{C}_{surf} + \mathcal{C}_{under} \\ \mathcal{C}_{surf}(x, y) > 0, \forall\ x, y \\ \mathcal{C}_{under}(x, y) > 0, \forall\ x, y \end{cases}$$

The results of this method are presented in Figure 4.5. They look smooth as expected. The separation is not complete and is again stuck in a local minimum. In Figure 4.6, we again compare the final solution found via gradient descent with the true separated sources. Again, we can observe

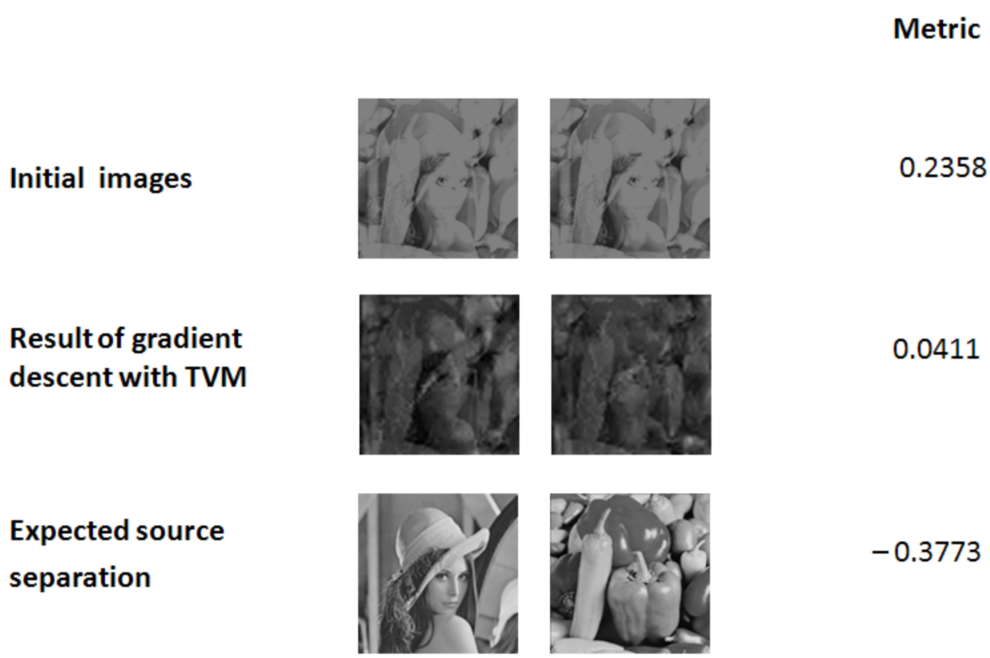

Figure 4.6: Comparison of the result of the gradient descent approach for the conditional entropy with total variation metric with the true separated sources.

that the gradient descent has clearly failed to get close to the true global minimum of the objective function.

To avoid getting stuck in local minima, initializing $\mathcal{C}_{surf}$ and $\mathcal{C}_{under}$ with random values is being attempted. Also, a multiresolution approach across various iterations is expected to help steer the algorithm away from getting stuck in local minima. These methods are currently being explored.

In summary, the chapter presents various attempts at source separation and their results using synthetic data. The methods presented are a very good start in attempting to achieve blind source separation. By adding methods to avoid local minima issues, the current results have the potential to converge successfully and separate the two sources completely.

Chapter 5

Identifying Areas of Information Loss

As discussed in the earlier chapters, X-ray synchrotron data may contain areas of information loss where a highly Xray-absorbent surface feature has blocked the signal from the underlayers from being imaged. Wavelet methods in [7] used to reconstruct these areas were discussed in Chapter 3. However the results are not as good as they ought to be and seem to indicate the need for more robust methods. A robust solution to determine the areas of no or partial information for inpainting is presented in this chapter.

Before arriving at the solution proposed in this thesis, numerous less successful methods were attempted. A discussion of these methods will give us a better perspective of the problem and also allow us to understand the progression of ideas that led to the solution presented here.

5.1 Enhanced Wavelet Method

The first attempt was to identify what had to be modified in the wavelet method [7]. The result in Figure 3.4 clearly shows that the separation into true and influence images is not complete. There are traces of the influence image on the true image obtained. The wavelet coefficients corresponding to the two components were expected to be separated well by the minimization procedure. Instead, it can be observed that even though the parent wavelets (coarser components of the image) were partitioned into the two components as expected; their child coefficients (finer components around them) did not always follow the pattern. We see a lot of a wavelet artifacts in the resulting images which are clearly caused by the finer wavelets not having filled in the peaks

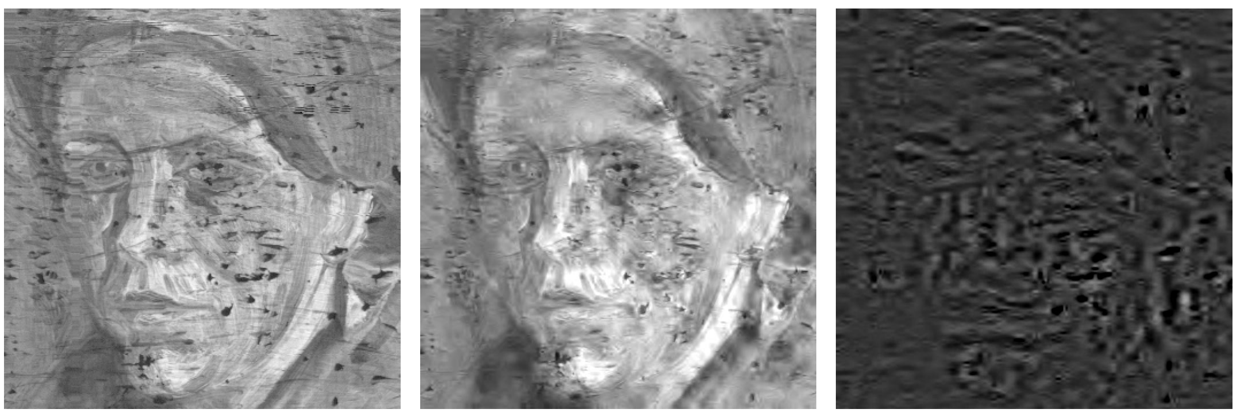

(a) Fixed, registered channel image. (b) True Image. (c) Influence Image.

Figure 5.1: Splitting of the channel image into true image and influence image for $\mu = 10$, $\nu = 15$, wavelet = db6, scale = 5 and number of iterations = 80.

and valleys in the larger wavelets properly. This disparity in the coefficients resulted in the residue of the influence image seen in the recovered underpainting.

To avoid this problem, the minimization problem had to be modified to encourage the child wavelets to follow the categorization decisions of the parent wavelets. The second and third term penalties were modified to be affected more by the parent wavelets rather than the children themselves. In this way, the categorization of child wavelets was biased to follow the categorization of their respective parents. This change was expected to pull in all the child wavelets along with their parent ones. The resulting minimization equation has now become

$$\sum |\mathcal{C}(\lambda) - (\mathcal{T}(\lambda) + \mathcal{I}(\lambda))|^2 + \sum \frac{\mu}{|\mathcal{I}(\lambda_{parent})|}\phi(\lambda)|\mathcal{I}(\lambda)|^2 + 2\nu \sum |\mathcal{I}(\lambda_{parent})||\mathcal{T}(\lambda)|$$

The solution for this equation can be obtained by iteratively solving the following equations

$$\mathcal{T}_n(\lambda) = \mathcal{S}_{\lambda|\mathcal{I}(\lambda_{parent})|}(\mathcal{C}(\lambda) - \mathcal{I}_n(\lambda))$$

$$\mathcal{I}_{n+1}(\lambda) = \frac{\mathcal{C}(\lambda) - \mathcal{T}_n(\lambda)}{1 + \frac{\mu}{|\mathcal{I}(\lambda_{parent})|}\phi(\lambda)}$$

The results obtained from this method appear to be more promising, but as can be seen in Figure 5.1, the sharpness and quality of the image are greatly compromised in this process. This negative effect could result from a majority of finer wavelet coefficients being assigned to the wrong category. The failure of these modifications led us to look for better solutions.

5.2 Contour Detection

Another method attempted was to detect the areas of information loss, which come in the form of either blobs where the surface painting contains flowers or thin streaks where the surface contains blades of grass, based on contour maps. As can be seen in the contour map of the channel image in Figure 5.2, contours of obstructions like blobs are closed ones. This pattern can be used as a metric in determining them. But due to the natural presence of many contours in an image, these obstructions can be specifically found by adding a few more conditions for their detection.

Let us take a look at how the holes in the image can be characterized. (1) It is visually evident that the blobs and blades are generally very much darker than their surroundings. (2) They are considerably big and prominent. (3) Also, it is typical that edges/contours of the blobs coincided with some edges on the surface image. These three conditions together should hence be able to identify almost all the obstructions.

To create the mask for inpainting using this method, all areas in the channel image which are darker than their surroundings were chosen. These areas were thresholded to be above at least 5 pixels wide so that only large dark patches were identified as obstructions. Specific hue ranges of the surface image were observed to be almost entirely corresponding to these large dark patches identified. By choosing the hue range 0.06 to 0.13, and selecting only the dark patches corresponding to this surface hue range, the edges of the mask obtained matched with edges on the surface image. The resulting mask obtained is shown in Figure 5.2.

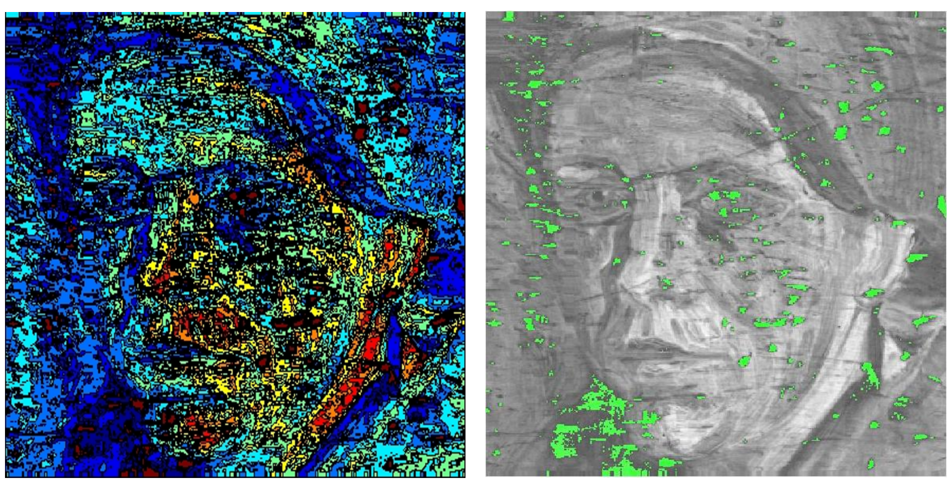

(a) Contour map of the Sb channel. (b) Detection of large areas of no information indicated by green color.

Figure 5.2: Contour approach results.

This process detected most of the large blobs effectively as can be verified from the results in Figure 5.2. It can be observed that all the brown-shaded contours of blobs which are bigger than a significant size are detected as obstructions by using this method.

The results look very encouraging as almost all the reasonably large size blobs were easily detected. But when the threshold for the size of the blob was reduced to include the smaller ones, there were an alarmingly high number of false positives. Also this method was not suitable to detect the blade-like obstructions which did not have definite contours most of the time. Results from Figure 5.2 also verify the fact that no blade-like obstructions were identified.

The approach was also heavily dependent on the visual analysis of the obstructions. Hence, there arose the need for a method which is not only independent of the prior knowledge of the surface image and underpainting, but can also be used to detect obstructions of any shape and size.

5.3 Hue Detection

5.3.1 Initial Examination

The search for an alternate solution led to taking a closer look at the channel and surface images. Observing the corresponding surface image, the losses were found to be highly correlated with a few specific types of surface features, in this case the yellow flowers and dark green grass blades. There are two possible reasons for this: (1) that these yellow and green strokes are particularly thick, or (2) that the pigments in these strokes are highly absorbent. We are unable to identify the true reason because these attributes always go together in this painting, as they would tend to in any Van Gogh painting. (See Figure 5.3 for a raking light photograph of the surface of “Pasture in Bloom”, demonstrating the thickness of various pigments on the surface layer.) However, regardless, we observe that there is a consistent relationship between surface color and loss of information in the underpainting. Hence, it seems possible that we might identify the areas in the underpainting in which information was lost using the surface hues as a guide.

Hence, in this section, we will first test this hypothesis that surface colors can be used to find nearly all areas of information loss. Our aim here is to find a range of hues on the surface that will identify virtually all darkened areas in the underpainting, to see if such a hue range actually exists. If this is true, then we will be justified in trying to develop a method to automatically identify these hues and inpaint the covered areas without any human intervention, which is our final goal.

We found that the hue ranges 0.06 to 0.13 and 0.7 to 1.0 in HSL color space, corresponding to yellow and green respectively, produce a reasonable mask for inpainting as shown in Figure 5.4. In the figure, the red pixels are those for which the surface hue was in the range 0.7 to 1.0, whereas the green pixels are those for which the surface hue was in the range 0.06 to 0.13.

Though the range selections were specific to this painting, it can be safely assumed that X-rays are differentially blocked by various hues and hence a hue-based detection mechanism could be a good candidate for a generic solution. The following section explains the hue-based automatic solution.

5.3.2 Automatic Hue Detection

While for this painting visual selection of hues was very clear, the idea is to develop an automatic hue identification procedure, so that we will be able to use it for other canvases that will typically present more complex problems, i.e. trying to solve Underpainting Recovery Stage 3 for general paintings.

To identify obstructing colors, the following method is proposed. Surface hues that are highly correlated with darkened areas in multiple chemical channels are to be identified. Thus, for each RGB color $\mathcal{C}$, the pixels of this color in the surface painting are applied as a mask to the chemical channel images. Then the average grayscale value of the masked-off region is compared with the average grayscale value in a small area surrounding it. Surface colors for which the masked-off region is significantly darker than its surroundings are likely attenuating. More precisely, for each color $\mathcal{C}$ and chemical element $\mathcal{E}$, the mean of the masked-off region is computed,

$$\tau_{\mathcal{C},\mathcal{E}} = \text{average}(\{I_{\mathcal{E}}(x,y) | I_{surface}(x,y) = \mathcal{C}\}),$$

where $I_{\mathcal{E}}$ is the image for chemical element $\mathcal{E}$ and $I_{surface}$ is the surface image, and that for the surrounding area

$$\rho_{\mathcal{C},\mathcal{E}} = \text{average}(\{I_{\mathcal{E}}(x,y) | I_{surface}(x,y) \neq \mathcal{C}, \text{ and } \exists x', y'$$

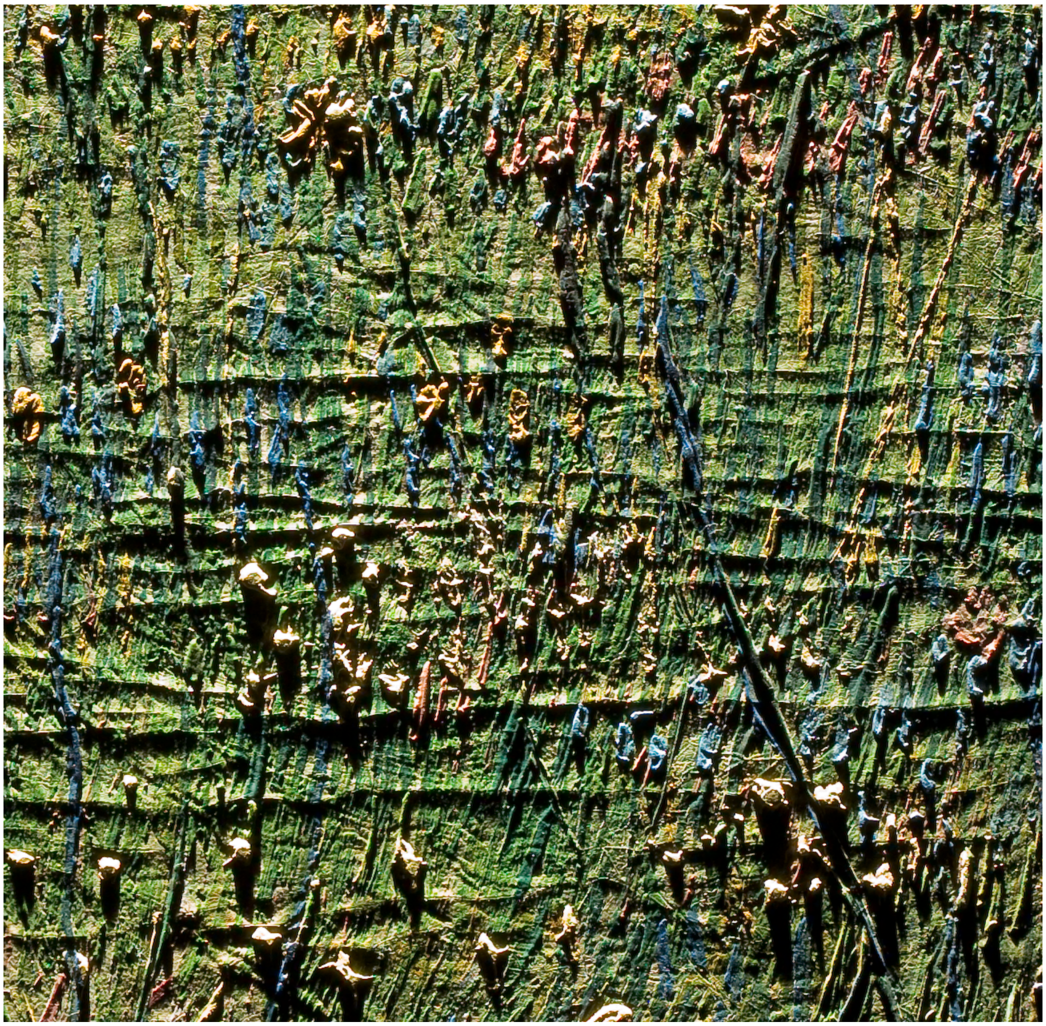

Figure 5.3: Raking light photograph of “Pasture in Bloom” demonstrating thickness of various pigments on surface layer.

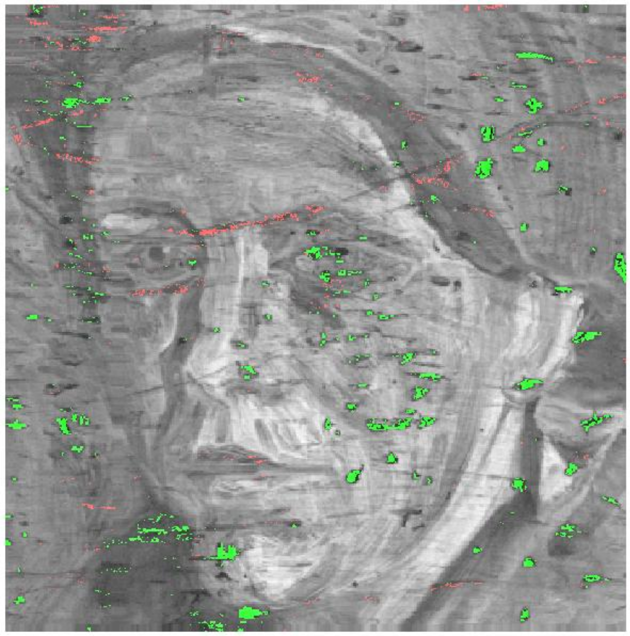

(a) Antimony channel image with estimated attenuation locations marked in green and red.

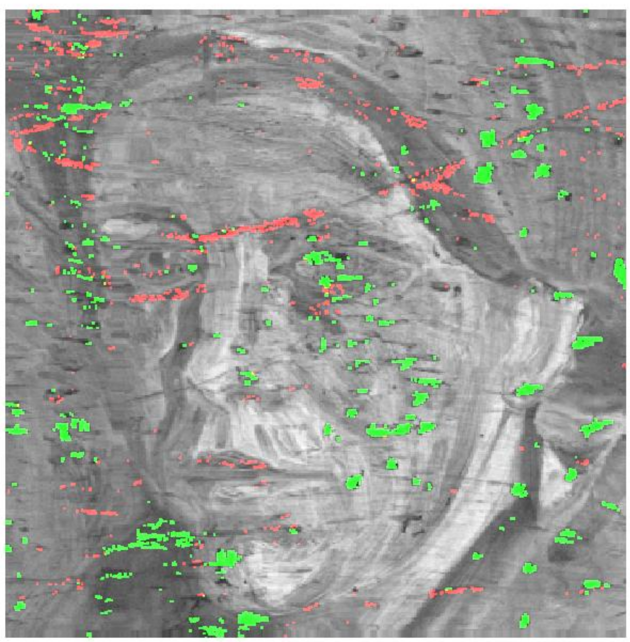

(b) An example mask for inpainting made from the estimated attenuation locations.

Figure 5.4: Result of simple attenuating hue identification procedure. Hue ranges 0.06 to 0.13 and 0.7 to 1.0 in HSL color space, corresponding to yellow and green respectively, produce a reasonable mask for inpainting.

(a) Antimony channel image.

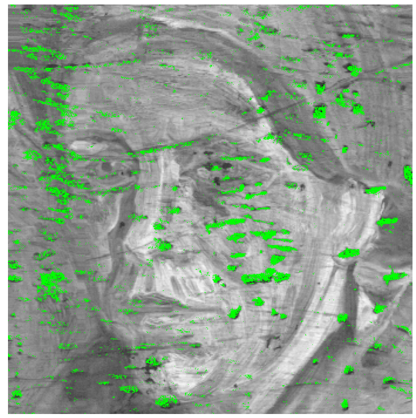

(b) Antimony channel image with estimated attenuation locations marked in green.

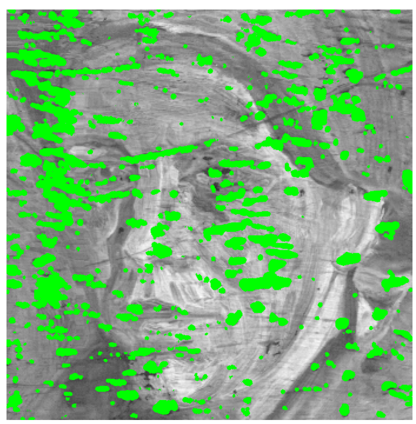

(c) An example mask for inpainting made from the estimated attenuation locations.

Figure 5.5: Results of the automated attenuating hue identification procedure.

$$\text{s.t. } \sqrt{(x'-x)^2+(y'-y)^2} \leq R,\ I_{surface}(x',y') = \mathcal{C}\})$$

for a given distance threshold R (50 pixels was used here). Then $\tau_{\mathcal{C},\mathcal{E}}$ and $\rho_{\mathcal{C},\mathcal{E}}$ are compared to determine whether the pixels under this surface color tend to be darker than the surrounding pixels. If the ratio $\frac{\rho}{\tau}$ exceeds a specified threshold (1.1 was used in this thesis) and ρ is sufficiently greater than 0, then this color $\mathcal{C}$ is considered to be attenuating.

Based on an exploratory analysis of the Van Gogh, selected shades of yellow, dark green, and occasionally pink were identified as those likely to have attenuated the underpainting signal. The first two colors, yellow and dark green, match human perception as was previously discussed. The pink is initially surprising, but on more careful inspection, we see darkened areas in the antimony channel corresponding to the pink flowers in the upper left corner of the surface patch. Using the chosen colors, we can produce a mask for inpainting, shown in Figure 5.5, by growing the selected region slightly. This pattern then covers most of the blackened or darkened areas in the image. To reduce the large size of the inpainting region, we would like to distinguish between complete and partial information loss in future work, so that regions of only partial loss can be repaired without discarding the information they retain.

5.4 Inpainting

An image inpainting algorithm developed in [4] was used as the baseline for inpainting the areas of information loss identified above. The choice of this implementation over [5] used by Brasoveanu et al. in [7] was because of the closeness of this algorithm to the manual inpainting process. In [4], Bertalmio et al. fills in masks in such a way that isophote lines arriving at the regions' boundaries are completed inside. This process is very similar to how a lost part of a painting will be inpainted manually by carrying forward lines from its boundaries. Details of the implementation can be found in [4]. By optimizing parameters in the method for this particular inpainting task, reasonable inpainting results were obtained for the masks derived earlier. As can be seen in Figure 5.6, the algorithm inpainted all of the spots detected to be inpainted by carrying over isophotic lines and hence looks very pleasing to the eye.

This chapter summarizes the various attempts at methods to identify areas of partial or little information on the source separated underpainting component image. The initial wavelet methods tried as an enhancement to previous works, though unsuccessful, laid the groundwork for the methods to follow, leading to the final proposed solution. The automatic hue detection method successfully detected almost all of the spots, except for a few blades and a blob by the eye, to be inpainted automatically. The result of inpainting these identified areas is also presented at the end, and looks very visually pleasing and plausible.

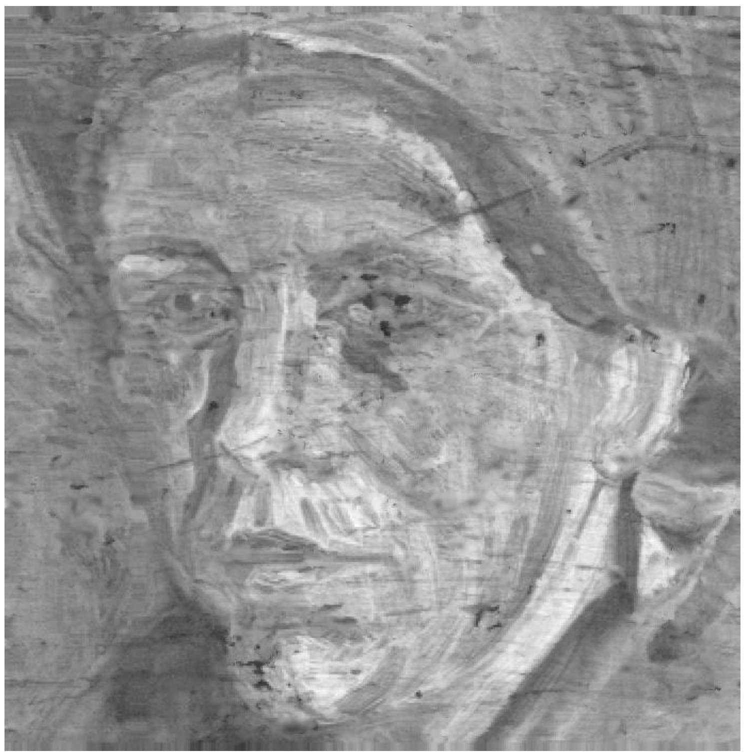

Figure 5.6: Result of inpainting the mask obtained by Automatic Hue Detection Method using the inpainting implementation in [4].

Chapter 6

Color Estimation from Chemical Element Data

This chapter will discuss Underpainting Recovery Stage 4 of the underpainting recovery process shown in Figure 1.6. The solution involves estimating the colors in the underpainting from the various chemical channel images. While we have called this problem “color estimation”, we note that it is typically not merely a problem of coloring a grayscale image. At the outset, we do not even possess a grayscale framework; instead, the known information is of various features of the painting that are spread across the multiple chemical element channels involved in producing their color (e.g. lips in one channel, eyes in another, etc.). Hence, what we have called “color estimation” is really a problem of how to combine all the different chemical element channels into one image, and is one of the most important and the most challenging subproblems of underpainting recovery.

The problem of color reconstruction is hard for many reasons. For one, the mapping from chemical element channel values to colors is complex and unknown. Colors are determined by a combination of chemical components and not having information about all the constituent components might prevent us from determining the exact color of a spot. Also, the fidelity of different channel information available can be different which may result in a bad estimate. Even the slightest difference in the proportion of constituents can predict an entirely different color for the original.

Moreover, the chemical values may not uniquely determine the color of the paint due to variation in response of various pigments to the imaging method. Not all colors can be imaged. For example, earth tone pigments such as brown are not imaged by the X-ray synchrotron imaging process, and thus browns are indistinguishable from other colors in our data. Thus, the problem is more than just a one to one mapping from a combination of available chemical information to a particular pigmentation estimate.

Finally, the presence of a pigment indicates the presence of that pigment at some depth on the canvas, but not necessarily at the surface of either the surface or underpainting. This means that all the edits that the artist made while creating the two paintings will be included in the available pigment information. But as our motive is to separate out just the finished underpainting's color, the additional information may lead to errors in our analysis.

To assess the feasibility of color estimation from chemical element channel images, we conducted a preliminary study in which we chose to work with a painting section for which we have some examples of the correspondences between chemical element concentrations and color.

6.1 Ribbon Reconstruction

In the Runge portrait previously mentioned, the presence of the purple ribbon around the girl's waist is indicated in the chemical element channels by mercury (Hg), present in Vermilion red, and cobalt (Co), present in Cobalt blue. The subtle changes in the shade of the ribbon are reflected in the chemical element channels, with more reddish purples containing more mercury and more bluish shades of purple containing more cobalt. Further examination of these two chemical element channels indicates that additional ribbons of a similar shade were previously present in the girl's hair. We can thus use the preserved ribbon at the waist to estimate the mapping from chemical elements to shades of purple in order to reconstruct the coloring of the missing ribbons.

The first stage is to register the channel images with the color image of the painting. Since this is a multimodal image registration problem, we proceed by choosing the transformation of the color surface image that maximizes the mutual information between the channel image and the color surface image. Mutual information as a term defines the amount of information (reduction in uncertainty) that knowing one random variable provides about another. Hence mutual information is maximum when both images are registered, and thus was chosen here as the metric for maximization. Histogram estimators were used to estimate the mutual information from the samples.

(a) Estimated hair ribbons (k = 50) superimposed on the portrait.

(b) Estimated hair ribbons in (a) superimposed on the Sb chemical channel showing the original hair.

(c) Closeup of waist ribbon on surface of painting.

(d) Waist ribbon with right half estimated from left half.

Figure 6.1: Results of k-nearest-neighbor estimation of colors from existing available training examples.

A brief overview of this method can be found in [12].

With the images aligned, we now estimate the mapping from the chemical element channels to colors. For simplicity, we begin by trying to find a mapping from the Hg and Co channels only since these red and blue pigments are the main chemicals that would be responsible for a purple color. We then proceed using a k-nearest-neighbor estimation. First, for every pixel j in the waist ribbon, the vector $x_j \in \mathbb{R}^2$ of its cobalt and mercury channel values, and the vector $y_j \in \mathbb{R}^3$ of its RGB values in the surface painting are stored as training examples. Now, given a new vector $x \in \mathbb{R}^2$ of the cobalt and mercury values for some new pixel, we estimate its RGB values $y \in \mathbb{R}^3$ as

$$y = \text{average}(\{y_j | x_j \text{ is one of the k nearest neighbors of } x\})$$

where "nearest" is defined as most similar in terms of Euclidean distance in $\mathbb{R}^2$.

Results of this procedure are shown in Figure 6.1. It can be seen that a reasonable color appears and that, like the waist ribbon, the hair ribbons show visually plausible evidence of shading with highlights appearing bluer and shadows appearing redder. Finally, as a sanity check we attempted to predict the right half of the waist ribbon based on the data available from the left half. The results show that the estimated waist ribbon is similar to the true ribbon.

The results for the purple ribbon in the subject's hair look very reasonable and realistic. Presence of the same color in another part of the painting and having complete chemical channel information for this color proved helpful in estimating the color with detailed shading. A more complex problem is to estimate the longer hair of the woman in the portrait as explained in the section below.

6.2 Hair Reconstruction

Though the long flowing hair of the subject in the Runge (Figure 6.2) is seen very distinctly in the lead and antimony channels, estimating its color is a far more challenging problem. The difficulty in estimation comes from the fact that the yellowish hue corresponding to the hair is represented by very few similarly colored pixels in the surface image, so we have very little training

(a) Pb channel.

(b) Sb channel.

Figure 6.2: Pb and Sb channels of the Runge painting showing clear traces of long hair underneath.

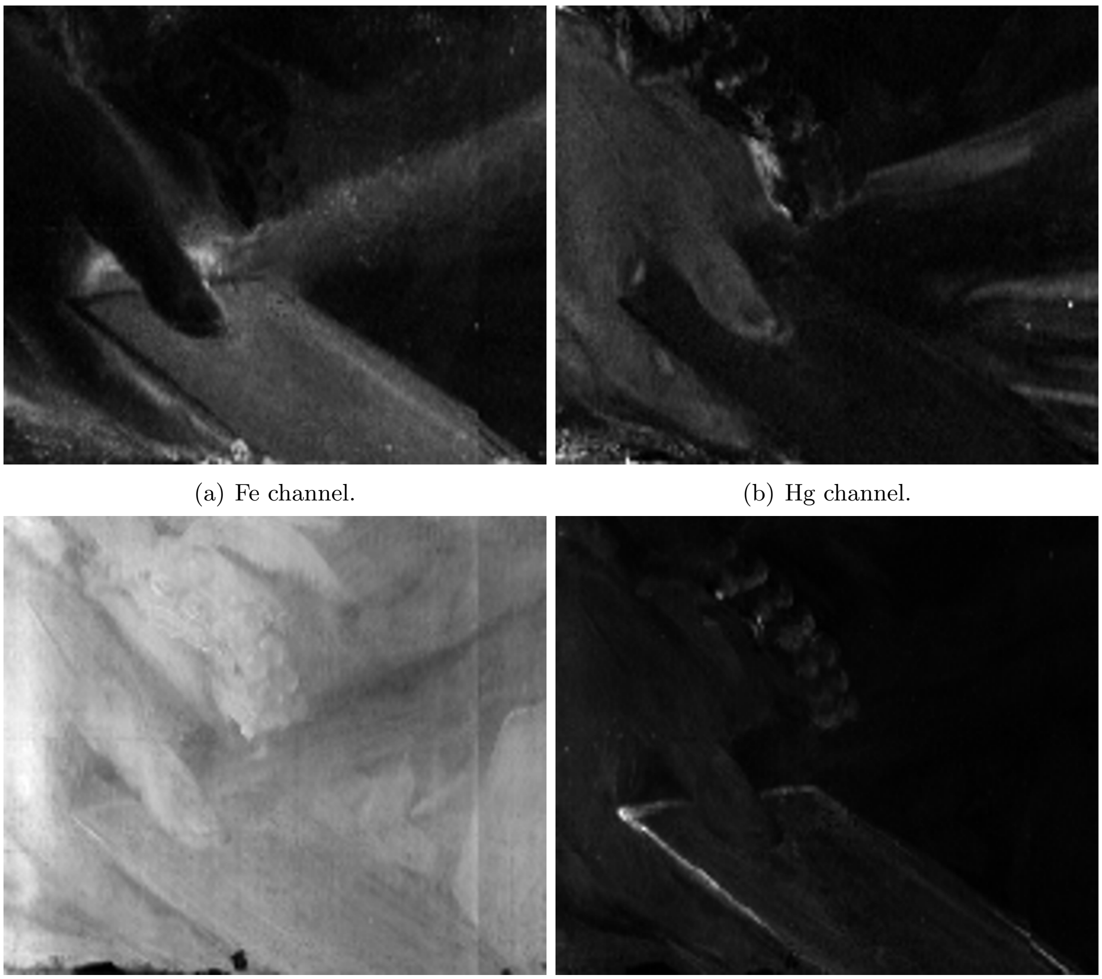

(a) Fe channel. (b) Hg channel.

(c) Pb channel. (d) Sb channel.

Figure 6.3: Channel images of the Runge painting's hand region.

data. The only yellowish region in the section of the portrait that was originally imaged are in the earrings which only cover a few pixels.

Fortunately, after the initial imaging was done on the portrait in Figure 1.4, the note in the subject's hand was suspected to have some writing on it. To get a closer look, the region around the hand holding the note was imaged again for more information. The data for some of the channels is shown in Figure 6.3. Though the new imaging data did not reveal any writing on the note, it gives some additional training data. The boundary around the note in her hand might also be of a similar color to the lost hair. Using both these sources of training data, we shall proceed with a regression analysis similar to that used for the ribbon.

The first step in this direction was to register the chemical channel data of the hand with the original digital portrait. Pb and Sb were the channels considered for this as these channels showed the most promising representation of the portrait's long flowing hair in the original imaging data. The resolution at which the main image and the hand region were imaged was different and hence the registration also involved finding the right scaling factor for maximizing mutual information. Histogram-based estimators were used as before for various scaling factors to arrive at the optimum registration for channel images. The lead channel was registered first using this method and the resulting alignment was also used for the Sb channel since it perfectly aligned with Pb.

After registration, we now map the chemical element channels to colors. As was done for the ribbon color estimation, for every pixel j in the yellow regions of the surface painting, the vector $x_j \in \mathbb{R}^2$ of its Sb and Pb channel values, and the vector $y_j \in \mathbb{R}^3$ of its RGB values in the surface painting are stored as training examples. Now, given a new vector $x \in \mathbb{R}^2$ of the Sb and Pb values for some new pixel, its RGB values $y \in \mathbb{R}^3$ are estimated as in the previous section. Due to higher variance in this data, smaller values of k are chosen for the nearest neighbor approach to give realistic results.

The results for this method do not look very promising. There are not many pixels which get colored a plausible cyellow. Most of them are brownish, presumably since brown pixels were present. Also, many non-hair pixels get substituted with these wrong brownish hues. This may be primarily because the original registered images were not registered closely enough and were not as identical across different channels as assumed. Even a slight change in the registration can offset the entire approach as the training data is very few in number. The causes for errors are being explored and analyzed.

Chapter 7

Conclusion

The thesis work presented a new generic approach to art restoration using data from synchrotron based X-ray fluorescence imaging. Two paintings by famous artists, Van Gogh and Runge, were scanned using the above-mentioned imaging technique.

The Van Gogh contained an entirely different painting hidden under the surface image. Chemical channel information of the painting, which revealed the underpainting, had a lot of artifacts due to various attenuating hues on the surface painting. These hues absorbed the X-rays even before they reached the lower layers where the underpainting is present, thereby destroying chemical channel information of the underpainting in these areas. The partial or little information in these attenuated areas has to be inpainted to recover the original underpainting. The identification of the areas to be inpainted is a critical step in this process and the development of an algorithm to do this was one of the main focuses of this thesis. The attenuating hue detection algorithm presented detects most areas of partial or complete information loss, and allows us to create a successful mask for inpainting. Our implementation is automated and is independent of the painting under study. This result provides the basis for further implementation on other paintings. In the future, we plan to extend the attenuating hue detection algorithm to distinguish between complete and partial information loss so that the partial information left in some areas can be used during the inpainting process.

The second painting studied is that of Phillipp Otto Runge, whose portrait of a woman revealed that the painting was altered to suit the social tastes of his time. The woman seemed to have had long flowing hair with ribbons adorning it and sported a dress with lower neckline under imaging light, very much unlike the conservative portrait of her in the surface image. The algorithm developed to estimate the color of the ribbons on her hair produced visually pleasing results with realistic shading effects and thus offers a method for estimating the colors of works of art.

An algorithm to solve the source separation problem of underpainting recovery was also attempted with synthetic data. Results were promising but not complete and future work is suggested to arrive at a better solution.

Art in its original form can never be replaced and restoration works can only get as close to the original, as margarine compares to delicious real butter. But such restoration helps us discover and enjoy pieces of art otherwise lost to eternity.

Bibliography

[1] A. Anitha and S. Hughes. Attenuating hue identification and color estimation for underpainting reconstruction from x-ray synchrotron imaging data. Proc. SPIE, Vol. 7798, 2010.

[2] M. Barni, F. Bartolini, and V. Cappellini. Image processing for virtual restoration of artworks. IEEE Multimedia, 7:34–37, Apr-Jun 2000.

[3] R. Berns, S. Byrns, F. Casadio, I. Fiedler, C. Gallagher, F. Imai, A. Newman, and L. Taplin. Rejuvenating the color palette of George Seurat's A Sunday on La Grande Jatte - 1884: A simulation. Color Res. & Appl., 31:278–293, 2006.

[4] M. Bertalmio and G. Sapiro. Image Inpainting. Proceedings of the 27th annual conference on Computer graphics and interactive techniques, 2000.

[5] S. Bhat. Object Removal by Exemplar-Based Inpainting. A CS7495 Final Project. Implementation of [1], MATLAB code available at http://www.cc.gatech.edu/sooraj/inpainting/, 2004.

[6] J. Blazek, B. Zitova, M. Benes, and J. Hradilova. Fresco Restoration: Digital Image Processing Approach. European Signal Processing Conference (EUSIPCO), 2009.

[7] A. Brasoveanu, I. Daubechies, S. Hughes, J. Dik, and K. Janssens. Uncovering a Lost Painting of Vincent van Gogh. Proceedings of SPIE Electronic Imaging: Computer Vision and Image Analysis of Art, 2010.

[8] A. Criminisi, P. Perez, and K. Toyama. Region filling and object removal by exemplar-based image inpainting. IEEE Trans. Image Proc., vol. 13, no. 9, pp. 1200, 2004.

[9] J. B. de la Faille. The Works of Vincent van Gogh: His Paintings and Drawings. Reynal & Company: Amsterdam, The Netherlands, 1970.

[10] J. Dik, K. Janssens, G. van der Snickt, L. van der Loeff, K. Rickers, and M. Cotte. Visualization of a Lost Painting by Vincent van Gogh Using Synchrotron Radiation Based X-ray Fluorescence Elemental Mapping. Analytical Chemistry, 80:6436–6442, 2008.

[11] M. Douma. Pigments through the Ages. http://www.webexhibits.org/pigments, 2008.

[12] X. Lu, S. Zhang, H. Su, and Y. Chen. Mutual information-based multimodal image registration using a novel joint histogram estimation. Computerized Medical Imaging and Graphics, Vol 32, 2008.

[13] H. Maitre, F. Schmitt, and C. Lahanier. 15 years of image processing and the fine arts. IEEE Int. Conference on Image Processing (ICIP), 1:557–561, 2001.

[14] N. Nikolaidis and I. Pitas. Digital image processing in painting restoration and archiving. IEEE Int. Conference on Image Processing (ICIP), 2001.

[15] E. Salerno, A. Tonazzini, and L. Bedini. Digital image analysis to enhance underwritten text in the Archimedes palimpsest. International Journal on Document Analysis and Recognition, 2010.

[16] X. Tang, P. A. Ardis, R. Messing, C. M. Brown, R. C. Nelson, P. Ravines, and R. Wiegandt. Digital Analysis and Restoration of Daguerreotypes. Proceedings of SPIE Electronic Imaging: Computer Vision and Image Analysis of Art, 2010.

[17] S. van Heugten. Radiographic Images of Vincent van Gogh's Paintings in the Collection of the van Gogh Museum. Van Gogh Museum Journal, 1995.

[18] S. Webber. Technical Imaging of Paintings. Williamstown Art Conservation Center Technical Bulletin, 2008.

[19] Y. Zhao, R. S. Berns, L. A. Taplin, and J. Coddington. An Investigation of Multispectral Imaging for the Mapping of Pigments in Paintings. Proceedings of SPIE Electronic Imaging: Computer Image Analysis in the Study of Art, 2008.